

1 **A full year of continuous net soil and ditch CO₂, CH₄, N₂O
2 fluxes, soil hydrology and meteorology for a drained fen in
3 Denmark**

4 Annelie S. Nielsen¹, Klaus S. Larsen¹, Poul Erik Lærke², Andres F. Rodriguez², Johannes
5 W.M. Pullens², Rasmus J. Petersen³, Jesper R. Christiansen¹

6 ¹Department of Geoscience and Natural Resource Management, University of Copenhagen, Frederiksberg, DK-
7 2000, Denmark

8 ²Department of Agroecology, Aarhus University, Tjele, DK-8830, Denmark

9 ³Department of Ecosystems and Natural Resource Management, Aarhus University, Aarhus, DK-8000, Denmark

10 *Correspondence to:* Jesper R. Christiansen (jrc@ign.ku.dk)

11 **Abstract.** We ~~here~~ present a detailed dataset (<https://doi.org/10.60612/DATADK/BZQ8JE>) of automated
12 greenhouse gas (GHG) net soil and ditch fluxes of carbon dioxide (CO₂), methane (CH₄), and nitrous oxide
13 (N₂O) from a drained fen in Denmark covering a full year. The dataset resolves small scale spatial and hourly-
14 daily-seasonal dynamics of GHG soil fluxes. The GHG flux dataset is accompanied by simultaneous time series
15 of soil temperature and moisture, as well as groundwater table depth and covers spatiotemporal gradients in soil
16 hydrological and climatic variability. The GHG fluxes of CO₂, CH₄ and N₂O were measured simultaneously by
17 a high-precision cavity ring down laser spectrometer connected with a novel automated GHG system platform
18 called SkyLine2D (Earthbound Scientific Ltd., UK) that allowed up to 27 individual chamber measurement
19 points along a 24 meter transect. In total 47.483 chamber measurements were completed and after quality
20 control 44.631 CO₂ fluxes, 44.099 N₂O and 42.515 CH₄ fluxes remained.

21 The average (\pm SE) net soil CO₂ efflux observed at the site ($2.6 \pm 0.02 \text{ } \mu\text{mol CO}_2 \text{ m}^{-2} \text{ s}^{-1}$ or $35 \pm 0.3 \text{ tCO}_2 \text{ ha}^{-1} \text{ y}^{-1}$)
22 aligns with findings from similar drained fens in northern Europe ~~covering. However, this transect average
23 masks substantial spatial variability and highlights the role of episodic emission bursts related to hydrological
24 variability.~~ The organic soil at the site was a larger net source of N₂O ($8.9 \pm 0.1 \text{ nmol N}_2\text{O m}^{-2} \text{ s}^{-1}$ or $123 \pm 1.4 \text{ kg
25 N}_2\text{O m}^{-2} \text{ ha}^{-1} \text{ y}^{-1}$) to the atmosphere compared to other temperate drained organic grassland soils in northern
26 Europe ~~with similar. The soil N₂O emissions were similarly spatial variability le in space as soil CO₂ effluxes.
27 However, the temporal variability of N₂O - fluxes were closely linked to fluctuations of the but were more
28 dynamic in time, where increasing groundwater table depth with in response to precipitation during warmer
29 seasons led to emission bursts of soil N₂O emissions during low water table depth. N₂O fluxes decreased that
30 dominated the annual net budget of soil N₂O and decreased to near-zero fluxes when the water table depth
31 increased in drier warmer periods.~~ Net soil CH₄ fluxes were near-zero and the site overall acted as a smaller net
32 source ($0.18 \pm 0.06 \text{ nmol CH}_4 \text{ m}^{-2} \text{ s}^{-1}$ or $0.91 \pm 0.3 \text{ kg CH}_4 \text{ ha}^{-1} \text{ y}^{-1}$) compared to other drained organic grassland
33 soils, although net uptake of atmospheric CH₄ was observed as well especially in drier conditions. ~~Compared to
34 the peat soil GHG fluxes, the ditch was a smaller net source of CO₂ ($0.94 \pm 0.05 \text{ } \mu\text{mol CO}_2 \text{ m}^{-2} \text{ s}^{-1}$ or $1.3 \pm 0.7
35 \text{ tCO}_2 \text{ ha}^{-1} \text{ y}^{-1}$) and N₂O ($0.35 \pm 0.03 \text{ nmol N}_2\text{O m}^{-2} \text{ s}^{-1}$ or $4.9 \pm 0.4 \text{ kg N}_2\text{O ha}^{-1} \text{ y}^{-1}$) to the atmosphere. The ditch
36 was also a net source of emission of CH₄ ($161 \pm 13 \text{ nmol CH}_4 \text{ m}^{-2} \text{ s}^{-1}$ or $812 \pm 66 \text{ kg CH}_4 \text{ ha}^{-1} \text{ y}^{-1}$) average of
37 diffusive and ebullition fluxes) to the atmosphere and annual cumulative emissions were was more than two
38 orders of magnitude larger than net the soil CH₄ emissions.~~

39 The very large number of fluxes of CO₂, N₂O and CH₄ for peat soils and a ditch linked to both groundwater
40 table data, soil moisture/temperature as well as groundwater and soil physicochemical parameters are unique to
41 northern temperate peatlands and holds a potential for exploring and testing basic hypothesis on the
42 simultaneous regulation of these gas fluxes by both soil hydrology and temperature, including soil and
43 groundwater chemistry. The high temporal detail also allows for time series analyses as well as investigations
44 into diurnal and seasonal patterns of fluxes in response to physical drivers. Similarly, the high frequency of
45 measured variables and the large number of spatial replicates are furthermore well suited for testing
46 biogeochemical models as it is possible to have both calibration and validation dataset covering the same period.
47 Furthermore, the surprisingly large spatial variability of flux data is ideal to include in model sensitivity tests
48 which can aid in constraining model outputs and develop model routines.

49 Diurnal and seasonal patterns of net soil CO₂ and N₂O emissions align with variations of soil temperature, but
50 no clear patterns were observed for net soil CH₄ uptake or emission. Compared to soil GHG fluxes, the ditch
51 was a smaller net source of CO₂ ($0.94 \pm 0.05 \text{ } \mu\text{mol CO}_2 \text{ m}^{-2} \text{ s}^{-1}$ or $1.3 \pm 0.7 \text{ } \text{CO}_2 \text{ ha}^{-1} \text{ yr}^{-1}$) and N₂O (0.35 ± 0.03
52 $\text{nmol N}_2\text{O m}^{-2} \text{ s}^{-1}$ or $4.9 \pm 0.4 \text{ kg N}_2\text{O ha}^{-1} \text{ yr}^{-1}$) to the atmosphere. The ditch was also a net source of CH₄ (161 ± 12
53 $\text{nmol CH}_4 \text{ m}^{-2} \text{ s}^{-1}$ or $812 \pm 66 \text{ kg CH}_4 \text{ ha}^{-1} \text{ yr}^{-1}$ average of diffusive and ebullition fluxes) to the atmosphere and
54 annual cumulative emissions were more than two orders of magnitude larger than net the soil CH₄ emissions,
55 confirming earlier findings that ditches can be CH₄ emission hotspots, where the ditch CH₄ is emitted in bursts
56 with little seasonal variability, including emissions as ebullitions.

57

58 The data set (<https://doi.org/10.60612/DATADK/BZQ8JE>) is well suited for testing and developing
59 biogeochemical models, with emphasis on the soil thermal hydrology interactions with the peat C and N cycles.

61 **1 Introduction**

62 Understanding the climate ~~feedbacksfeedback~~ of temperate drained and rewetted wetlands requires robust
63 observational datasets of net fluxes, e.g. whether the rewetted peatlands act as net sources to the atmosphere or
64 sinks of greenhouse gases (GHG). This necessitates being able to capture spatial and temporal variability from
65 these systems. Flux data covering all three major GHGs are rare for temperate peatlands, and despite growing
66 efforts to quantify GHG fluxes from drained peatlands, existing datasets often suffer from limited temporal
67 resolution, short monitoring periods, or a lack of concurrent hydrological and meteorological data. Many studies
68 rely rely on manual chamber-based measurements or short term campaigns that may be able to fail to capture
69 overall seasonal dynamics, but fail to capture short term transient emission phenomenon in response to
70 fluctuations in physical drivers, for example fluctuating groundwater and extreme events. Also, manual based
71 measurements are labour intensive limiting the number of spatial replicates. Moreover, current high temporal
72 resolution datasets for wetlands using eddy covariance typically offer either high good quality temporal
73 resolution (e.g., eddy covariance or automatic chambers) for a specific wetland site, but it is challenging to
74 derive the specific spatial variability across the different sub-environments within the wetland, for example
75 between hummocks and hollows with different GHG emission profiles, with poor spatial coverage, or manual
76 measurements with good spatial resolution but very low temporal frequency. This discrepancy between spatial
77 and temporal coverage of current flux methodologies in wetlands in turn this hampers the ability to develop
78 precise models that integrate spatiotemporal patterns and can forecast GHG fluxes at the ecosystem scale more
79 precisely. This can impact the ability to predict, and hence climatic ~~feedbacksfeedback~~ of wetlands now and
80 under future alteration of these systems driven by, in these systems under land use and climatic changes.

81 However, automated GHG closed chamber flux measurements from ecosystems are becoming increasingly
82 common, also in peatland research (Anthony and Silver, 2023; Boonman et al., 2024) as equipment costs
83 decrease and awareness grows about the importance of resolving temporal variability of GHG fluxes to better
84 understand soil biogeochemical processes and soil-climate feedback. But high-frequency data of GHG fluxes
85 are still scarce for peatlands and spatial variability of fluxes is rarely represented as well due to limited number
86 of spatial replicates. Thus, most automated chamber systems are setup around a multiplexer control unit linking
87 multiple chambers with one or more GHG analysers. State-of-the-art automatic chamber systems, like the LI-
88 8250 Automated Gas Flux System (LiCOR, USA) or the eosAC-LT/LO (Eosense Inc. Canada), i.e. allow for a
89 standard number of 8 or 16 chambers, respectively, that can be upgraded to 36 chambers with additional
90 manifolds. Such large replicate chambers allow for improved characterization of spatial variation or treatment
91 effects coupled with temporal ~~variations, but~~variations but are costly to establish.

92 ~~Additionally, the introduction of automated chamber systems raises the need for improved data handling and~~
93 ~~flux calculation tailored to handle a wide range of flux magnitudes and chamber behaviour or design. Recent~~
94 ~~examples of novel flux calculation software are based on publicly available R codes and include goFlux, HMR,~~
95 ~~and fluxfinder. Furthermore, unsupervised automated chamber flux measurements increases the likelihood of~~
96 ~~misinterpretation of fluxes, such as overestimated night time fluxes due to atmospheric stratification that~~
97 ~~disturbs the steady state diffusion gradient between soil and the atmosphere or leaky chambers that disturb~~
98 ~~chamber headspace concentrations. This is a significant challenge of automated chamber systems producing~~

99 thousands of data points, where manual control of each data point may not be practical or feasible calling for
100 automated and objective quality control such as used with the eddy covariance methodology.

101 We here present a dataset that addresses the abovementioned limitations by uniquely combining high-frequency,
102 continuous measurements of net soil fluxes of carbon dioxide (CO₂), methane (CH₄) and nitrous oxide (N₂O)
103 with detailed hydrological and meteorological variables. The GHG fluxes were measured with an automated
104 GHG, called SkyLine2D, chamber system over 12 months resolving spatiotemporal patterns of GHG fluxes
105 including 27 individual collars (26 on organic soil and 1 in a ditch) over a 24 m transect on a temperate drained
106 fen peatland. Integrated quality control, flagging of erroneous or uncertain flux measurements enabled objective
107 filtering of poor quality data on the entire dataset. This comprehensive spatiotemporal coverage
108 enables robust calibration and validation of biogeochemical and hydrological models, particularly those aiming
109 to simulate the complex interactions between water table dynamics, soil processes, and GHG emissions in
110 managed peatland systems.

111 Considering the critical need for obtaining high-quality data on soil GHG fluxes from natural and restored
112 peatlands in Europe and globally, our dataset marks an important contribution to this endeavour as it addresses
113 current data shortcomings for Danish and European peatlands by providing detailed data on temporal and spatial
114 patterns of GHG fluxes from organic soils and drainage ditches together with environmental drivers of soil
115 hydrology and temperature, organic soil properties and groundwater geochemistry. We publish this data with the
116 aim of it being used by the scientific community for both experimentalists to test hypothesis of how GHG
117 dynamics are related to hydrology, soil, geochemistry and climate, as well as for the modelers to test and
118 develop biogeochemical models for peat lands.

119 2 Materials and Methods

120 2.1 Site description and the SkyLine2D system

121 The field site, Vejrumbro (N 56.43819 E 9.54527 (WGS 84)), is located in Central Jutland, in Denmark near the
122 city of Viborg (Fig. 1A) with a mean annual temperature of 8.3°C and annual precipitation of 675 mm for the
123 period 1991–2020 (measured 6 km away at Aarhus University Viborg Meteorological Station in Foulum
124 (Jørgensen et al., 2023)). It is situated in the Nørre Å valley and is characterized as a riparian fen peat soil (Reza
125 Mashhadi et al., 2024). The riparian fen developed in a former glacial river valley with flat topography gently
126 sloping (<2.5 meters over 300 meters) towards the Nørre Å that forms the central river in this area (Fig. S1).
127 The site was drained in 1950 with ditches and tile drains for cultivation but and has was primarily served used to
128 cut hay for fodder as as grassland in recent decades due to the the conditions were unfavourable for cereal
129 production wet conditions (Nielsen et al., 2024). Since 2018, Vejrumbro has been a living lab for
130 agroecological research managed by the Department of Agroecology at Aarhus University. From 2018, the site
131 had a passive rewetting strategy by terminating maintenance of the open ditches. During 2022, the main ditches
132 were gradually blocked.

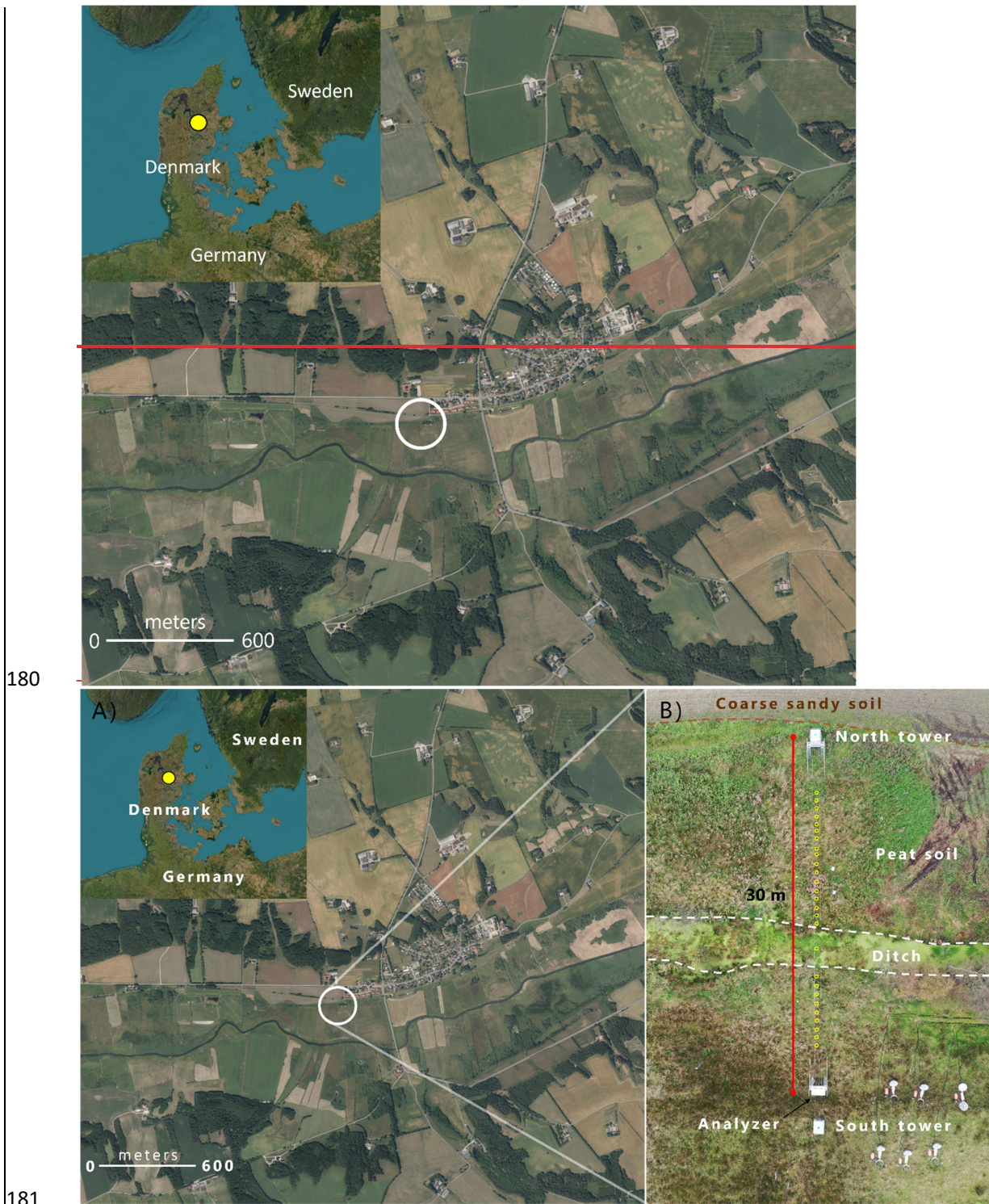
133 2.1.1 Site preparation and disturbance

134 Initially, we chose to perform the flux measurements without aboveground plants as the small chamber
135 dimensions (height of 20 cm) prohibited inclusion of these in the chamber as the plants typically reach over 100

136 cm in height at this site. The strategy was therefore to focus on measuring net soil GHG fluxes, where we
137 assume the contribution of gases are derived from heterotrophic respiration of older peat C/N, root exudated
138 C/N from adjacent plants, dissolved N in groundwater and belowground autotrophic respiration (CO_2) from
139 roots inhabiting the peat below the collars. We are aware that omitting plants prohibit a full evaluation of the net
140 ecosystem exchange of GHG and hence its net climate impact, as the aboveground plants represent a net sink of
141 atmospheric CO_2 ~~and also and~~ can increase the emission of CH_4 and N_2O (Jørgensen et al., 2012; Vroom et al.,
142 2022). However, by ~~avoiding removing~~ plants we ~~also~~ isolate the soil processes leading to net soil
143 emission/uptake of the GHG ~~and resolve spatiotemporal patterns to a higher degree than previous studies at this~~
144 ~~site have achieved and what other commercial platforms are capable of~~. Collectively, this can provide a
145 mechanistic insight into the regulation of fluxes by hydrology and temperature. We acknowledge that ~~future~~
146 studies of GHG fluxes in peatlands should seek to include the aboveground plant component to the net GHG
147 flux from the ecosystem if possible.

148 Two months prior to collar installation in summer 2021, we cleared vegetation within and around each collar
149 ($\sim 40 \times 40$ cm) by harvesting and applying a single recommended dose of glyphosate ($\sim 100 \text{ mg m}^{-2}$) to
150 aboveground plants only, avoiding soil contact. Glyphosate's average half-life in mineral soils is ~ 21 days,
151 ranging from 6–87 days and increasing with clay content (Padilla and Selim, 2020). Given the low dose and
152 absence of clay, residual glyphosate was likely minimal during flux measurements. Although repeated
153 applications can suppress microbial activity (Nguyen et al., 2016), the single treatment months prior suggests
154 limited direct impact on microbial respiration. Still, transient effects cannot be ruled out, and the lack of an
155 untreated control prevents quantification. Regrowth inside collars was manually removed at least weekly,
156 minimizing photosynthetic CO_2 uptake. While regrowth abundance was not measured, stable net CO_2 efflux
157 between removals suggests minimal impact. Aboveground plant removal is standard for isolating soil GHG
158 fluxes, though belowground autotrophic respiration from adjacent roots remained, as trenching was avoided to
159 reduce site disturbance. Without a control plot, the direct effect of disturbance on GHG fluxes remains
160 uncertain. The disturbance to the transect related to initial harvesting and removal of aboveground plants and
161 continuous removal of aboveground live plant inside the collars and in a small perimeter outside the collar. In
162 this way we kept an approximate area of 40×40 cm clear of vegetation at each collar. Two months prior to
163 installation of collars in summer of 2021, the transect (Fig. 2) was harvested and remaining living aboveground
164 vegetation was killed by applying one recommended dose of glyphosate ($\sim 100 \text{ mg m}^{-2}$) to the plants only across
165 the transect and avoiding spraying on the soil surface. The half-life of labile glyphosate in mineral soils range
166 between 6–87 days (average 21 days) with clay contents increasing half-life. The absence of clay and low
167 dosage indicate that there were no, or only little traces of glyphosate left once the flux measurements began and
168 hence the glyphosate treatment likely did not have a direct impact on the measured fluxes. Continued glyphosate
169 application would potentially have reduced microbial activity in the soil and thus lower microbial respiration.
170 Considering that we sprayed the vegetation only one time with glyphosate months prior to flux measurements,
171 we assume the direct impact on soil microbial processes to be small. However, we cannot fully rule out that
172 glyphosate may have led to a transient response. Because we did not have an undisturbed control we cannot
173 quantify the effects of glyphosate. Subsequently, regrowth inside the collars was restricted by manual harvesting
174 of emerging plants at a minimum of once every 7 days and throughout the period. Plant removal from collars is
175 considered a common practice to isolate net soil GHG fluxes as the aboveground autotrophic respiration is

176 removed. Since the individual collars were not trenched it is unavoidable to include belowground autotrophic
177 respiration from plants growing adjacent to the collars. To avoid excessive disturbance of the site we did not
178 remove these roots. Since we did not have a control, untreated/unharvested plot it is not possible to assess the
179 direct impact of the disturbance on the GHG fluxes.



182 **Figure 14: A)** The Vejrumbro location in Jutland (N 56.43819 E 9.54527 (WGS 84)) in the Nørre Å valley near the
 183 village of Vejrumbro. The grey circle marks the placement of the SkyLine2D system. Satellite images: © Google
 184 Earth. **B)** Drone image of the measurement transect (September 27th, 2023) after flux measurements had stopped.
 185 Dashed brown line marks the approximate boundary between the agricultural field, coarse sandy soil (north) and the
 186 peat/organic soil (south). The red line marks the end points of the SkyLine2D system (30 meters). The open yellow
 187 circles (n=27) mark the approximate position of individual collars across the transect of the field (24 meters in length)

188 where greenhouse gas fluxes were measured. The ditch is located between the dashed white lines. The analyser was
189 placed at the south tower. Elevation above sea level along the 24-meter collar transect varied from 3.77 m in the south
190 to 4.06 m in the north.

191 **2.22 Overview of time series of GHG fluxes, soil temperature/moisture, air temperature, wind direction**
192 **and groundwater level**

193 The dataset is comprised of a 12-month time series of net soil fluxes of CO₂, CH₄ and N₂O, accompanied by a
194 longer timeseries of soil temperature and moisture at 5 cm depth, meteorological variables (air temperature,
195 wind speed and direction measured at 2 meter height) and a shorter time series groundwater table level, depth
196 and temperature (Fig. 3, Table 21). Due to equipment failure of the SkyLine2D the GHG flux measurements
197 started on February 2nd, 2022 and ended January 28th, 2023 in total 360 days (Table 21). Groundwater level
198 measurements started between March 9th to 31st, 2022 (Table 1). All other variables were measured continuously
199 from July 1st, 2021, until January 31st, 2023 (Table 1). In the period between December 7th and 19th, 2022
200 intermittent periods of snow cover (depth was not measured) on the ground occurred. This snow cover did not
201 impede flux measurements.

202

Table 1: Available time series data from the Vejrumbro SkyLine2D system. Coloured time periods in 2021 to 2023 for each variable indicate data availability.

Variable	Unit	Model/sensor type	Data availability												2023					
			2021			2022			2023											
			Aug	Sep	Oct	Nov	Dec	Jan	Feb	Mar	Apr	May	Jun	Jul	Aug	Sep	Oct	Nov	Dec	Jan
CO ₂ flux*	μmol CO ₂ m ⁻² s ⁻¹	G2508 (Picarro Inc., USA)	~10**																	
CH ₄ flux*	nmol CH ₄ m ⁻² s ⁻¹	G2508 (Picarro Inc., USA)	~10**																	
N ₂ O flux*	nmol N ₂ O m ⁻² s ⁻¹	G2508 (Picarro Inc., USA)	~10**																	
Soil temperature at 5 cm depth***	°C	RXW-TMB-868 (Onset, USA)	5																	
Soil water content at 5 cm depth***	(cm ³ cm ⁻³)	RXW-SMD-868 (Onset, USA)	5																	
Air temperature at 2 m height	°C	S-TIC-M002 (Onset, USA)	5																	
Wind speed	m s ⁻¹	S-WSB-M003 (Onset, USA)	5																	
Wind direction	°	S-WDA-M003 (Onset, USA)	5																	
Groundwater level****	m.a.s.l.	DCL532 (BD sensors, Germany)	15																	
Groundwater table depth****	cm	DCL532 (BD sensors, Germany)	15																	
Groundwater temperature ****	°C	Dallas DS 18B20	15																	

*Net soil/ditch fluxes for all collars 1 - 27.

**Time in between two consecutive flux measurements. The 10 minutes comprise actual flux measurement of 5 minutes and 5 minutes headspace flushing between flux measurements.

***Measured for a subset of collars: 4, 7, 9, 23, 27.

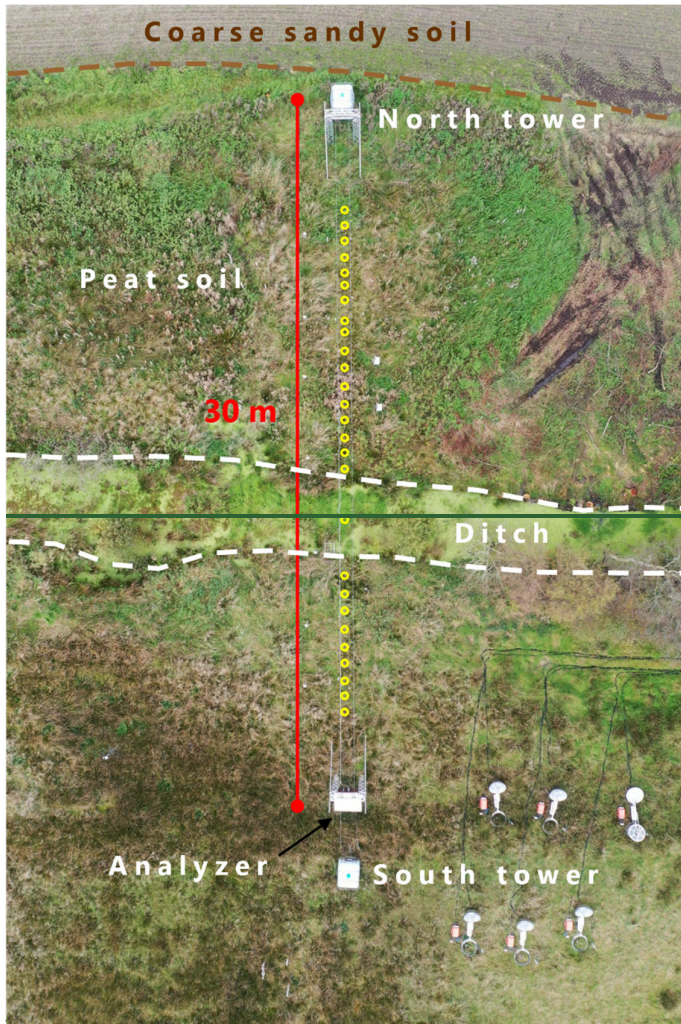
****Measured for a subset of collars: 1, 5, 10 (ditch), 13, 18, 22, 27.

203

204

205

206



207
 208 Figure 2: Drone image of the measurement transect (September 27th, 2023) after flux measurements had stopped.
 209 Dashed brown line marks the approximate boundary between the agricultural field, coarse sandy soil (north) and the
 210 peat/organic soil (south). The red line marks the end points of the SkyLine2D system (30 meters). The open yellow
 211 circles (n=27) mark the approximate position of individual collars across the transect of the field (24 meters in length)
 212 where greenhouse gas fluxes were measured. The ditch is placed between the dashed white lines. The analyser was
 213 placed at the south tower. Elevation above sea level along the 24 meter collar transect varied little from 3.77 m in the
 214 south to 4.06 m in the north.

215 **2.1.4.3 The SkyLine2D system configuration at Vejrumbro**

216 The SkyLine2D system is an automated chamber based system for measuring GHG fluxes. The system is
 217 designed and built by Earthbound Scientific Ltd. (United Kingdom). We used the SkyLine2D system to measure
 218 the net soil fluxes of carbon dioxide (CO_2), methane (CH_4) and nitrous oxide (N_2O) measured with an automated
 219 GHG chamber system over 12 months resolving spatiotemporal patterns of GHG fluxes including 27 individual

220 collars (26 on organic soil and 1 in a ditch) over a 24 m transect on a temperate drained fen peatland (Fig. 1B
221 and 3).

222 The SkyLine2D system transect was oriented in a north-south direction (Fig. 21B). Two 2.5 meter tall 2.5-
223 meter-tall scaffold towers marked the end of the 30 m SkyLine2D system (Fig. 21B and Fig. S2D). The towers
224 were fixed by ropes attached to 1000L pallet tanks filled with water (Fig. S2D) that maintained a stable position
225 of the towers and ropes and hence placement of the chamber over the collars. The measurement transect was in
226 total 24 m with 27 individual measurement collars for GHG fluxes on the ground, 26 on organic soil and 1 in a
227 drainage ditch (Fig. 2 and 3). The GHG analyser (model G2508, Picarro Inc., USA) was installed in a
228 waterproof and temperature-controlled shelter at the south end of the transect (Fig. 21B and Fig. S2C). The
229 transect was situated on the edge of the riparian fen in close proximity to near the mineral upland soils, where
230 active agriculture was practiced (Fig. 1B2). Along the transect volumetric soil water content (SWC) and soil
231 temperature (ST) as well as water table depth (WTD) were measured at seven locations (Fig. 24). The
232 agricultural field north of the SkyLine2D was sown with annual crops in rotation according to normal common
233 practice.

234 2.3.1.6 Greenhouse gas flux measurements with the SkyLine2D system at Vejrumbro

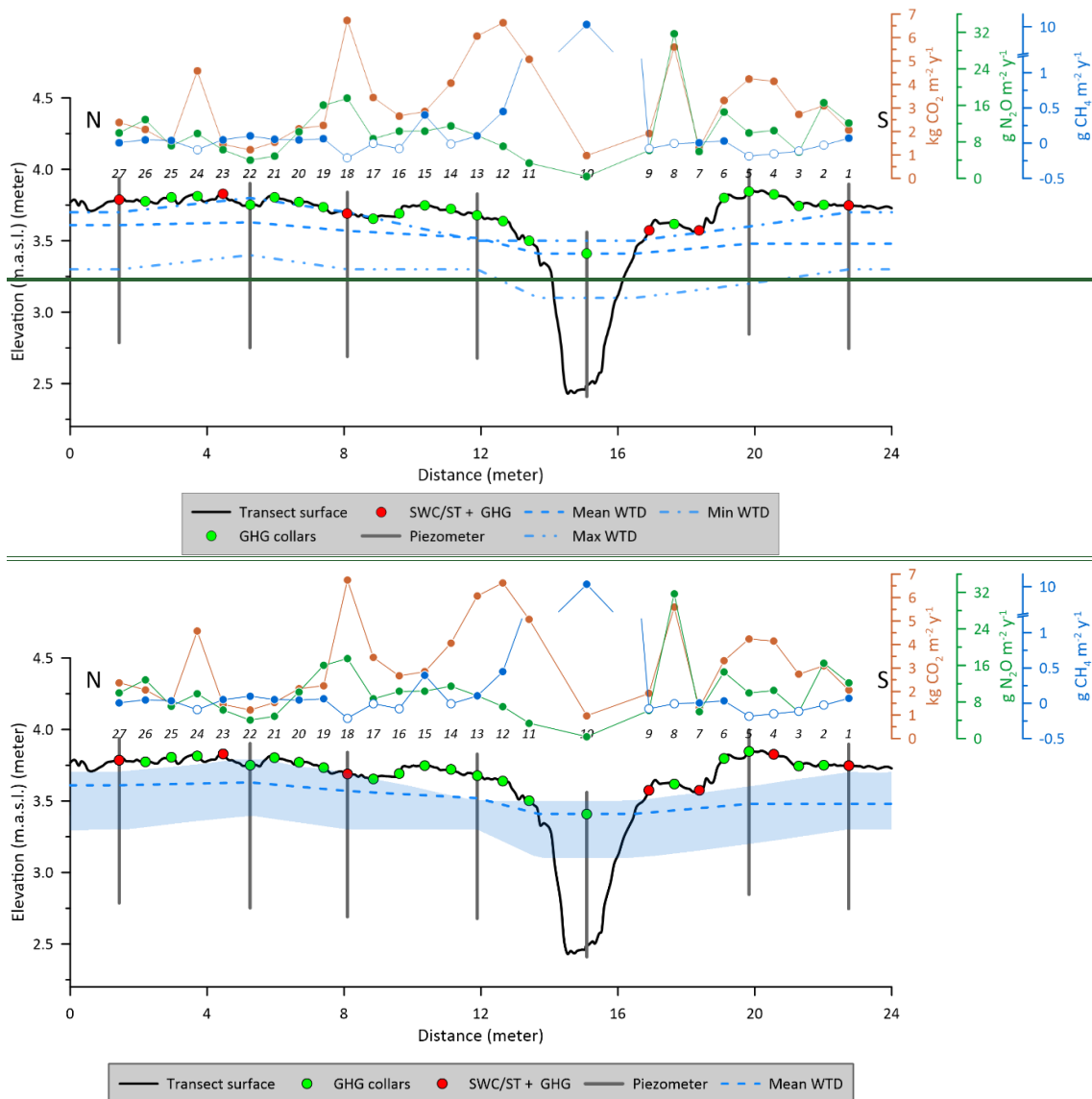
235 Along the SkyLine2D transect the 26 individual collars (Ø19 cm) along the 24 meter meters transect on organic
236 soil (Fig. 2) were inserted 5 cm into the peat leaving 5 cm above the surface. The collars were distanced app. 70
237 cm apart. One collar was installed in the ditch by inserting a tube (Ø19 cm, length 100 cm) to the bottom of the
238 ditch with holes deeper than the minimum water level in the ditch to allow water flow. Thus, it was avoided that
239 air entered in the collar in the ditch due to low water levels in the ditch. On top of this longer tube a collar (Ø19
240 cm, length 10 cm) was glued allowing for flux measurements. The chamber was programmed to stop when the
241 bottom of the chamber sat the water surface if the water level in the ditch extended above the top of the collar.
242 For most of the time the collar was not submerged, and the chamber therefore hit the collar.

243 There was one round transparent chamber (height: 39.5 cm and inner Ø: 19 cm, volume: 11.2 L) on the
244 SkyLine2D, hanging below a moving trolley, which was suspended on two ropes stretched between the north
245 and south towers (Fig. S2A and B). At defined positions along the rope, neodymium magnets had been inserted,
246 and a magnet sensor (Fig. S2B) on the trolley informed the internal computer to stop and lower the chamber
247 over positions with a collar on the surface. The chamber was lowered and guided down to the collar by
248 supporting rods shaping a funnel (Fig. S2A). The chamber stopped when it hit the collar, achieved through a
249 pressure sensor on top of the chamber connected to a hollow rubber gasket (Ø 3 cm) at the bottom, which also
250 sealed the chamber with the collar. There was no fan installed in the chamber as the mixing was ensured by the
251 main pump (Fig. S2C). A vent was installed in the top of the chamber to allow for pressure equilibration under
252 windy conditions and chamber deployment.

253 One entire flux + flushing sequence lasted 10 minutes (Table 1). The chamber closure period was set to 5
254 minutes with a purging time of 5 minutes in between measurements when chamber was open and hanging
255 underneath the trolley at approximately 1 meter above the ground (Fig. S2D). This provided on average 10 min
256 between flux measurements on consecutive collars (Table 1). Due to small variations in mechanical operations,
257 flux measurements were occasionally farther apart than 10 minutes, but overall, the timing of the SkyLine2D

258 system was consistent. After each cycle of 27 flux measurements there was a 30-minute delay until the start of
259 the next cycle. On average this resulted in 4-5 flux measurements per collar per day throughout the period.

260 To determine the concentrations of CO_2 , CH_4 and N_2O in the chamber air, a laser spectroscopy GHG analyser
261 (model G2508, Picarro Inc., USA) was used. The sample output frequency was set to 1 Hz with a manufactured
262 specified raw precision on 1 Hz data for CO_2 : 240 ppb, CH_4 : 0.3 ppb and N_2O : 5 ppb at ambient conditions
263 (Picarro Inc., USA). A main pump (model: N86 KN.18, KNF, Germany) circulated the air to and from the
264 chamber at 6 L min^{-1} . The GHG analyser was installed in parallel to the inflow from the chamber due to the
265 much lower flow of 250 mL min^{-1} of the vacuum pump. There was a 30-meter tube between the chamber and
266 main pump to allow for the GHG analyser to remain stationary in the hut while the trolley moved.



267
268 **Figure 2: Schematic representation of the measurement transect at Vejrumbro and associated measurement**
269 **variables. The annual cumulative fluxes of CO_2 (red) ($\text{kg CO}_2 \text{ m}^{-2} \text{ v}^{-1}$), N_2O (green) ($\text{g N}_2\text{O m}^{-2} \text{ v}^{-1}$) and CH_4 (blue) (g**
270 **$\text{CH}_4 \text{ m}^{-2} \text{ v}^{-1}$) are shown for each collar across the measurement transect at Vejrumbro. Closed and open symbols for**
271 **CH_4 represent net cumulative emission and uptake, respectively. Mean groundwater level is the mean water table**

273 elevation measured in piezometers (blue dashed line) with shaded blue area represent maximum and minimum
274 observed groundwater elevation. GHG collars (green symbols) mark the positions of greenhouse gas flux
275 measurements of CO₂, CH₄ and N₂O. SWC/ST + GHG mark the positions where volumetric soil water content
276 (SWC) and soil temperature (ST) at 5 cm depth were measured alongside greenhouse gas fluxes. Numbers on top of
277 plot show the collar numbers (from 1 – 27). N and S mark the north and south ends of the transect (see Fig. 1B). The
278 peat depth was at least one meter in all points. Elevation is given meters above sea level (m.a.s.l.).

279 Figure 3: Schematic representation of the measurement transect at Vejrumbro and associated measurement
280 variables. The annual cumulative fluxes of CO₂ (red) (kg CO₂ m⁻² y⁻¹), N₂O (green) (g N₂O m⁻² y⁻¹) and CH₄ (blue) (g
281 CH₄ m⁻² y⁻¹) are shown for each collar across the measurement transect at Vejrumbro. Closed and open symbols for
282 CH₄ represent net cumulative emission and uptake, respectively. Mean WTD is the mean water table depth measured
283 in piezometers (blue dashed line). GHG collars (green symbols) mark the positions of greenhouse gas flux
284 measurements of CO₂, CH₄ and N₂O. SWC/ST + GHG mark the positions where volumetric soil water content
285 (SWC) and soil temperature (ST) at 5 cm depth were measured alongside greenhouse gas fluxes. Numbers on top of
286 plot show the collar numbers (from 1 – 27). N and S mark the north and south ends of the transect (see Fig. 3). The
287 peat depth was at least one meter in all points.

288

289 **2.1.24 Peat and organic soil characteristics sampling and analysis**

290 In November 2023 the peat across the SkyLine2D transect was sampled to 1 meter depth using a Russian auger
 291 and cores split into five layers of 20 cm thickness. Collars 1, 2, 5, 6, 8, 13 – 27 were sampled (Fig. 2). For the
 292 remaining collars it was not possible to retrieve a sample due to excessive wetness of the peat. The
 293 decomposition of the peat samples were assessed by a 10-point Von Post scale of humification (1 = completely
 294 undecomposed and 10 = completely decomposed) together with quantification of the $\text{pH}_{\text{H}_2\text{O}}$ determined by
 295 suspending peat in demineralized water (1:5 peat:water mix), dry bulk density (g cm^{-3}) and total C and N by
 296 dry combustion ($\text{g C/N 100 g peat}^{-1}$ or %) (Table 1).

297 **Table 1 Mean (\pm standard error of the mean (SE)) peat/organic soil characteristics of humification degree (Von Post),
 298 $\text{pH}(\text{H}_2\text{O})$, dry bulk density (ρ_{dry}), total C (TC) concentration, total N concentration (TN) and the C/N ratio for collars
 299 1, 2, 5, 6, 8 and 13 – 27 at the Vejrumbro transect.**

Depth (cm)	N	Von post		$\text{pH}(\text{H}_2\text{O})$		$\rho_{\text{dry}}(\text{g cm}^{-3})$		TC (%)		TN (%)		C/N	
		Min	Max	Mean	\pm SE	Mean	\pm SE	Mean	\pm SE	Mean	\pm SE	Mean	\pm SE
0–20	20	7	10	4.2	0.08	0.31	0.02	26	1.1	1.6	0.06	16	0.4
20–40	20	5	10	4.6	0.06	0.20	0.01	43	1.3	1.8	0.04	24	0.7
40–60	11	3	8	4.9	0.10	0.15	0.01	48	1.8	1.9	0.05	25	1.1
60–80	11	3	6	5.3	0.09	0.11	0.01	47	1.8	1.9	0.05	24	0.6
80–100	10	4	8	5.4	0.09	0.10	0.02	44	2.1	1.9	0.05	24	0.6

300 Generally, there was peat/organic soil to one meter depth except for one collar (25) where gytta was found in a
 301 depth of 80 cm (Table 1). The organic soil was more decomposed in the top 40 cm indicated by higher Von Post
 302 values between 5 and 10. Below 40 cm peat still displayed high levels of decomposition along the transect, but
 303 was more often found to be less decomposed, values ranging from 1–8 (Table 1). This corresponds well to the
 304 previous land use with drainage of the topsoil leading to higher degree of humification. Also, the organic soil
 305 was most dense in the top 20 cm (on average $0.31 \pm 0.02 \text{ g cm}^{-3}$) and bulk density decreased to 0.10 – 0.12 g cm^{-3}
 306 from 40–100 cm depth. Total C and N was lowest in the 0–20 cm layer, but still classified as organic soil.
 307 Below 20 cm total C and N concentrations, respectively were similar. C/N ratio was lowest in the top 20 cm
 308 (16 ± 0.4) and increased to 22 – 25 in 20–100 cm depth (Table 1).

309 **2.4.5 Groundwater table level, and depth and sampling**

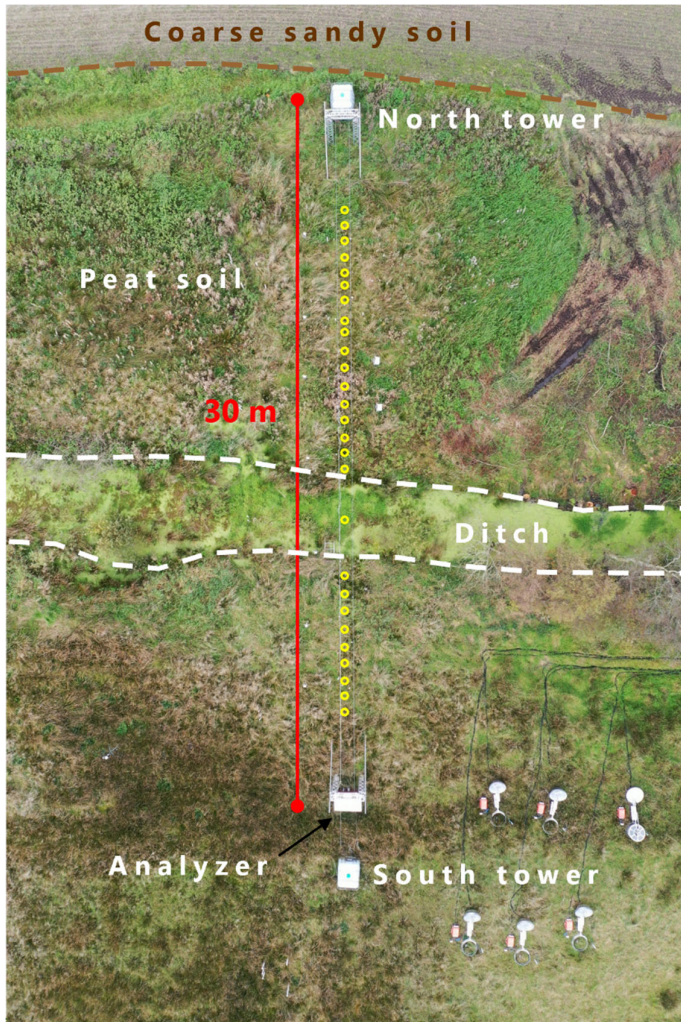
310 To measure the groundwater level Piezometers (inner diameter 5 cm) were installed at collars 1, 5, 10 (ditch),
 311 13, 18, 22, 27 (Fig. 4.2) to 1 meter depth below the surface, which is deeper than the lowest groundwater
 312 level in summer (~60 cm below the surface) with openings from 0.1–1.2 meter below terrain. In the ditch the
 313 piezometer bottom was deeper than one meter to secure anchoring in the peat. The piezometers were installed
 314 approximately 50–60 cm beside the collars to avoid interference with the SkyLine2D system. After installation,
 315 piezometers were cleaned and sealed at the surface with bentonite pellets to avoid surface infiltration along the
 316 piezometers which can distort water level measurements.

317 Pressure transducers (Table 12) connected to Arduino-loggers were installed in each piezometer (at collars 1, 5,
 318 10, 13, 18, 22 and 27 – Fig. 3.2) approximately 1 m below terrain measuring water levels every 15 minutes. The
 319 pressure transducers were vented and thus do not need correction for atmospheric pressure.

320 The groundwater levels were described using two metrics: hydraulic head and groundwater table depth
321 (GWD WTD). Hydraulic head represents the water level relative to mean sea level, based on the Danish Vertical
322 Reference (DVR90), while GWD WTD indicates the depth of the groundwater below the surface terrain and
323 represented in positive values, where WTD of zero is equivalent to groundwater level at the terrain surface. The
324 elevation of top of the piezometers were measured using a GPS (model GS07 High Precision GNSS Antenna
325 with a CS20 Controller, Leica, Germany) and used as a local reference for hydraulic head. Manual
326 measurements of groundwater levels were conducted every 2 months and used to calibrate the logger water
327 levels to hydraulic head and GWD WTD.

328 2.5.1.3 Groundwater water sampling and chemical analysis

329 Groundwater was sampled monthly in the piezometers placed at collars 1, 5, 13, 18, 22 and 27 (Fig. 32) by
330 retrieving a 200 mL sample 20-30 cm below the groundwater level at the sampling time. The water sample was
331 retrieved using a syringe and transferred to a plastic bottle that was capped immediately to avoid exchange with
332 the atmosphere and air bubblescontamination. Water samples were frozen immediately after sampling and
333 subsequently after thawing analyzed for pH, EC and alkalinity on ~~an~~ 855 Robotic Titrosampler (Metrohm,
334 Germany). Total N and DOC were measured on a TOC-V CPH Analyzer with Total Nitrogen Unit TNM-1 &
335 ASI-V Autosampler (Shimadzu, Japan). Ion chromatograph (IC) analyses of Cl⁻, NO₃⁻, and SO₄²⁻ were
336 performed on a 930Compact IC Flex (Metrohm, Germany) and NH₄⁺ concentrations were measured with
337 continuous flow analysis using a Seal AA500 Autoanalyzer (SEAL Analytic, USA). Total dissolved Fe and P
338 were analyzed with coupled plasma–mass spectrometry (ICP-MS) on an iCAP-Q ICP-MS (Thermo Fisher
339 Scientific, USA) in KED mode using He as the collision gas. Prior to analysis the 10 mL subsamples were
340 acidified with 200 μ L concentrated nitric acid ~~to a 10 mL sample~~. Elemental ICP-MS analyses also included
341 dissolved base cations of Ca²⁺, Mg²⁺, K⁺, Na⁺ as well as total dissolved Al and Mn cations (not ~~shown~~,
342 ~~but~~shown but included in the data set).



343

344 **Figure 2.** Drone image of the measurement transect (September 27th, 2023) after flux measurements had stopped.
 345 Dashed brown line marks the approximate boundary between the agricultural field, coarse sandy soil (north) and the
 346 peat/organic soil (south). The red line marks the end points of the SkyLine2D system (30 meters). The open yellow
 347 circles (n = 27) mark the approximate position of individual collars across the transect of the field (24 meters in length)
 348 where greenhouse gas fluxes were measured. The ditch is placed between the dashed white lines. The analyser was
 349 placed at the south tower. Elevation above sea level along the 24 meter collar transect varied little from 3.77 m in the
 350 south to 4.06 m in the north.

351

2.1.4 SkyLine2D system configuration at Vejrumbro

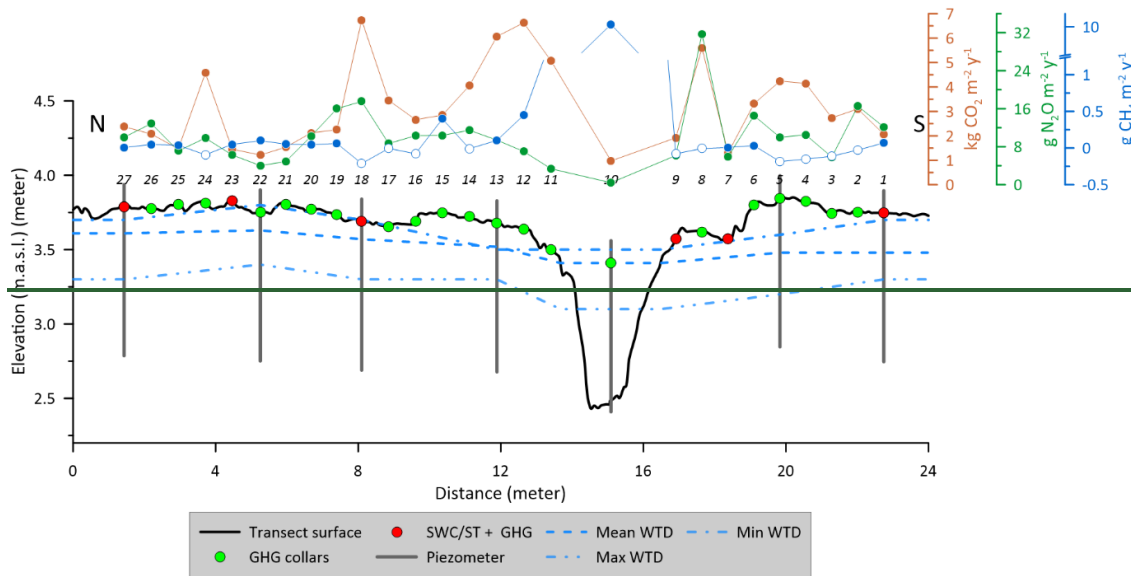
352

The SkyLine2D system is an automated chamber based system for measuring GHG fluxes. The system is
 353 designed and built by Earthbound Scientific Ltd. (United Kingdom). We used the SkyLine2D system to measure
 354 the net soil fluxes of carbon dioxide (CO_2), methane (CH_4) and nitrous oxide (N_2O) measured with an automated
 355 GHG chamber system over 12 months resolving spatiotemporal patterns of GHG fluxes including 27 individual
 356 collars (26 on organic soil and 1 in a ditch) over a 24 m transect on a temperate drained fen peatland.

357

The SkyLine2D system transect was oriented in an north-south direction (Fig. 2). Two 2.5 meter tall scaffold
 358 towers marked the end of the 30 m SkyLine2D system (Fig. 2 and Fig. S2D). The towers were fixed by ropes

359 attached to 1000L pallet tanks filled with water (Fig. S2D) that maintained a stable position of the towers and
 360 ropes and hence placement of the chamber over the collars. The measurement transect was in total 24 m with 27
 361 individual measurement collars for GHG fluxes on the ground, 26 on organic soil and 1 in a drainage ditch (Fig.
 362 2 and 3). The GHG analyser (model C2508, Picarro Inc., USA) was installed in a waterproof and temperature
 363 controlled shelter at the south end of the transect (Fig. 2 and Fig. S2C). The transect was situated on the edge of
 364 the riparian fen in close proximity to the mineral upland soils, where active agriculture was practiced (Fig. 2).
 365 Along the transect volumetric soil water content (SWC) and soil temperature (ST) as well as water table depth
 366 (WTD) were measured at seven locations (Fig. 4). The agricultural field north of the SkyLine2D was sown with
 367 annual crops in rotation according to normal practice.



368
 369 **Figure 3.** Schematic representation of the measurement transect at Vejrumbro and associated measurement
 370 variables. The annual cumulative fluxes of CO_2 (red) ($\text{kg CO}_2 \text{ m}^{-2} \text{ y}^{-1}$), N_2O (green) ($\text{g N}_2\text{O m}^{-2} \text{ y}^{-1}$) and CH_4 (blue) ($\text{g CH}_4 \text{ m}^{-2} \text{ y}^{-1}$) are shown for each collar across the measurement transect at Vejrumbro. Closed and open symbols for
 371 CH_4 represent net cumulative emission and uptake, respectively. Mean WTD is the mean water table depth measured
 372 in piezometers (blue dashed line). GHG collars (green symbols) mark the positions of greenhouse gas flux
 373 measurements of CO_2 , CH_4 and N_2O . SWC/ST + GHG mark the positions where volumetric soil water content
 374 (SWC) and soil temperature (ST) at 5 cm depth were measured alongside greenhouse gas fluxes. Numbers on top of
 375 the plot show the collar numbers (from 1–27). N and S mark the north and south ends of the transect (see Fig. 3). The
 376 peat depth was at least one meter in all points.
 377

378 **2.2 Overview of time series of GHG fluxes, soil temperature/moisture, air temperature, wind direction and 379 groundwater level**

380 The dataset is comprised of a 12-month time series of net soil fluxes of CO_2 , CH_4 and N_2O , accompanied by a
 381 longer timeseries of soil temperature and moisture at 5 cm depth, meteorological variables (air temperature,
 382 wind speed and direction measured at 2 meter height) and a shorter time series groundwater table level, depth
 383 and temperature (Fig. 3, Table 2). Due to equipment failure of the SkyLine2D the GHG flux measurements
 384 started on February 2nd, 2022 (Table 2). Groundwater level measurements started between March 9th to 31st,
 385 2022 (Table 1). All other variables were measured continuously from July 1st, 2021, until January 31st, 2023.

386 (Table 1). In the period between December 7th and 19th, 2022 intermittent periods of snow cover (depth was not
387 measured) on the ground occurred. This snow cover did not impede flux measurements.

388 **2.3.6 Soil moisture and temperature measurements**

389 Soil moisture and temperature probes were initially inserted for ~~was measured at~~ collars 1, 4, 7, 9, 18, 23, 27
390 (Fig. ~~are~~ 42) in order to obtain a representation of the entire transect, and ~~Soil moisture~~ probes (6 cm length)
391 were inserted at an approximate 30° angle 5 cm outside the collar, while the soil temperature probes were
392 inserted vertically adjacent to the soil moisture probe. Due to sensor failures soil moisture was measured for
393 collars 1, 7, 9, 18, 23 and 27 and soil temperature at 4, 7, 9, 23 and 27.

394 **2.4 Groundwater table level and depth**

395 ~~Piezometers (inner diameter 5 cm) were installed at collars 1, 5, 10 (ditch), 13, 18, 22, 27 (Figure 4) to 1 meter~~
396 ~~depth below the surface, which is deeper than the lowest groundwater level in summer (~60 cm below the~~
397 ~~surface) with openings from 0.1–1.2 meter below terrain. In the ditch the piezometer bottom was deeper than~~
398 ~~one meter to secure anchoring in the peat. The piezometers were installed approximately 50–60 cm beside the~~
399 ~~collars to avoid interference with the SkyLine2D system. After installation, piezometers were cleaned and~~
400 ~~sealed at the surface with bentonite pellets to avoid surface infiltration along the piezometers which can distort~~
401 ~~water level measurements.~~

402 ~~Pressure transducers (Table 2) connected to Arduino loggers were installed in each piezometer (at collars 1, 5,~~
403 ~~10, 13, 18, 22 and 27 (Fig. 3) approximately 1 m below terrain measuring water levels every 15 minutes. The~~
404 ~~pressure transducers were vented and thus do not need correction for atmospheric pressure.~~

405 ~~The groundwater levels were described using two metrics: hydraulic head and groundwater depth (GWD).~~
406 ~~Hydraulic head represents the water level relative to mean sea level, based on the Danish Vertical Reference~~
407 ~~(DVR90), while GWD indicates the depth of the groundwater below the surface terrain. The elevation of top of~~
408 ~~the piezometers were measured using a GPS (model GS07 High Precision GNSS Antenna with a CS20~~
409 ~~Controller, Leica, Germany) and used as a local reference for hydraulic head. Manual measurements of~~
410 ~~groundwater levels were conducted every 2 months and used to calibrate the logger water levels to hydraulic~~
411 ~~head and GWD.~~

412 **2.5.7 Wireless data transfer**

413 Wireless sensors for air temperature, wind speed, wind direction, soil temperature and volumetric soil water
414 content were set up with Wi-Fi data transfer to HOBO RX3000 Weather Station (Onset, USA) equipped with
415 HOBOnet Manager (RXMOD-RXW-868) module for wireless communication with sensors and logged data
416 every 5 minutes. Data access was through the HOBOlink cloud software.

417 Groundwater loggers were interfaced with the I²C (Inter-integrated Circuit) protocol and data was collected on
418 Arduino custom-built logger (<https://vandstande.dk/logger.php>) with wireless connection via LoRaWAN or
419 SigFox.

420 **2.6 Greenhouse gas flux measurements with the SkyLine2D system at Vejrumbro**

421 ~~Along the SkyLine2D transect the 26 individual collars (Ø19 cm) along the 24 meter transect on organic soil~~
422 ~~(Fig. 3) were inserted 5 cm into the peat leaving 5 cm above the surface. The collars were distanced app. 70 cm~~
423 ~~apart. One collar was installed in the ditch by inserting a tube (Ø19 cm, length 100 cm) to the bottom of the~~

424 ~~ditch with holes deeper than the minimum water level in the ditch to allow water flow. Thus, it was avoided that~~
425 ~~air entered in the collar in the ditch due to low water levels in the ditch. On top of this longer tube a collar (Ø10~~
426 ~~cm, length 10 cm) was glued allowing for flux measurements. The chamber was programmed to stop when the~~
427 ~~bottom of the chamber sat the water surface if the water level in the ditch extended above the top of the collar.~~
428 ~~For most of the time the collar was not submerged and the chamber therefore hit the collar.~~

429 There was one round transparent chamber (height: 39.5 cm and inner Ø: 19 cm, volume: 11.2 L) on the
430 ~~SkyLine2D, hanging below a moving trolley, which was suspended on two ropes stretched between the north~~
431 ~~and south towers (Fig. S2A and B). At defined positions along the rope, neodymium magnets had been inserted,~~
432 ~~and a magnet sensor (Fig. S2B) on the trolley informed the internal computer to stop and lower the chamber~~
433 ~~ever positions with a collar on the surface. The chamber was lowered and guided down to the collar by~~
434 ~~supporting rods shaping a funnel (Fig. S2A). The chamber stopped when it hit the collar, achieved through a~~
435 ~~pressure sensor on top of the chamber connected to a hollow rubber gasket (Ø 3 cm) at the bottom, which also~~
436 ~~sealed the chamber with the collar. There was no fan installed in the chamber as the mixing was ensured by the~~
437 ~~main pump (Fig. S2C). A vent was installed in the top of the chamber to allow for pressure equilibration under~~
438 ~~windy conditions and chamber deployment.~~

439 ~~One entire flux + flushing sequence lasted 10 minutes (Table 1). The chamber closure period was set to 5~~
440 ~~minutes with a purging time of 5 minutes in between measurements when chamber was open and hanging~~
441 ~~underneath the trolley at approximately 1 meter above the ground (Fig. S2D). This provided on average 10 min~~
442 ~~between flux measurements on consecutive collars (Table 1). Due to small variations in mechanical operations,~~
443 ~~flux measurements were occasionally farther apart than 10 minutes, but overall, the timing of the SkyLine2D~~
444 ~~system was consistent. After each cycle of 27 flux measurements there was a 30 minute delay until the start of~~
445 ~~the next cycle. On average this resulted in 4.5 flux measurements per collar per day throughout the period.~~

446 ~~To determine the concentrations of CO₂, CH₄ and N₂O in the chamber air, a laser spectroscopy GHG analyser~~
447 ~~(model G2508, Picarro Inc., USA) was used. The sample output frequency was set to 1 Hz with a manufactured~~
448 ~~specified raw precision on 1 Hz data for CO₂: 240 ppb, CH₄: 0.3 ppb and N₂O: 5 ppb at ambient conditions~~
449 ~~(Picarro Inc., USA). A main pump (model: N86 KN 18, KNF, Germany) circulated the air to and from the~~
450 ~~chamber at 6 L min⁻¹. The GHG analyser was installed in parallel to the inflow from the chamber due to the~~
451 ~~much lower flow of 250 mL min⁻¹ of the vacuum pump. There was a 30 meter tube between the chamber and~~
452 ~~main pump to allow for the GHG analyser to remain stationary in the hut while the trolley moved.~~

453 **2.7.8 Calculation of diffusive fluxes**

454 Fluxes were calculated and quality checked using the goFlux R package (Rheault et al., 2024) and presented as
455 $\mu\text{mol CO}_2 \text{ m}^{-2} \text{ s}^{-1}$, $\text{nmol N}_2\text{O m}^{-2} \text{ s}^{-1}$ and $\text{nmol CH}_4 \text{ m}^{-2} \text{ s}^{-1}$. Prior to flux calculations, the gas concentration data
456 from the G2508 analyzer was matched to the chamber closure time and chamber id in order to determine the
457 start time of the chamber measurement, so it was possible to separate individual flux measurements from each
458 collar over the measurement time (see examples of flux detection and calculation in Fig. S3A-D). An automatic
459 deadband detection method was applied based on maximal R^2 of a linear regression over the first 180 s (in 10 s
460 steps) after chamber closure. The deadband was allowed to attain values between 0 to 150 seconds thereby also

461 allowing for compensation for the ~60 s delay between chamber headspace gas concentration change and GHG
462 analyser detection due to transport time through the 30 m tube connecting the chamber and GHG analyser.

463 Flux calculations were done with both linear (LM) and non-linear (Hutchinson-Mosier – HM) regression models
464 (Pihlatie et al., 2013) to determine the slope at time zero. The best flux estimates with either the LM or HM
465 regression model was determined using the *best.flux* function in the goFlux package (Rheault et al., 2024).
466 Shortly, if the RMSE of the HM model was lower than minimum detectable flux (MDF), HM was chosen.
467 However, if the ratio (g-factor) between HM and LM was larger than 2, LM was chosen, as this indicates over-
468 fitting of the HM, which may result in unrealistic large HM flux estimates. If the relative SE of the slope
469 (SE/slope) at time zero for the HM model was larger than 100% it indicated overfitting of the HM model and
470 the LM was chosen. This approach is conservative as it will discard non-linear flux behaviour and instead
471 provide a conservative linear flux estimate. Out of 47.438 detected flux measurements for CO₂, CH₄ and N₂O,
472 respectively, a total of 2807 CO₂ fluxes (5.9%), 3339 N₂O fluxes (7%) and 4923 CH₄ fluxes (10.3%) were
473 discarded ~~either~~ due to the following two situations: 1) chamber mechanical malfunction ~~either resulting in~~
474 ~~imperfect sealing on collar due to erroneous lowering of chamber on collar indicated by background~~
475 ~~atmospheric or fluctuating gas concentrations in the headspace~~~~and 2) –at in situ flux levels close to the~~
476 ~~minimum detectable flux of the Picarro G2508 analyser~~ (Christiansen et al., 2015) ~~At low flux levels~~ non-
477 significant ~~regression (between concentration and time and GHG concentration) (p>0.05) fluxes~~ were ~~also~~
478 discarded as it was not possible to ~~statistically visibly detect distinguish~~ whether there was a ~~real~~ flux ~~due to high~~
479 ~~noise signal ratio of the analyser and/or the lack of significant regression it was because of the~~ chamber ~~had~~
480 ~~malfunctioned.~~ It is acknowledged that discarding low fluxes can bias annual means and cumulative values, but
481 the data quality did not allow us to determine whether the flux measurement was performed correctly and hence
482 a conservative approach was chosen as including false low fluxes would also bias the data set.

483 For flux measurements the air temperature in 2 meters was used as an estimate of the chamber headspace
484 temperature along with a 1 atm air pressure.

485 The annual cumulated fluxes from the soil or the ditch (diffusive only) were estimated simply by multiplying the
486 daily average CO₂, CH₄ or N₂O flux for the measurement period with 365 days. We believe for the purpose of
487 data presentation that this simplistic methodology is adequate here, also given the very few data gaps in the
488 timeseries. However, there are other more sophisticated methods using interpolation and response variable
489 functions that may refine the annual budget. However, it is not the goal of this manuscript to present these
490 methodologies but to provide the data so other users can test different temporal upscaling methodologies.

491 **2.8.9 Calculation of ebullition fluxes in the ditch**

492 Methane ebullition fluxes were occasionally observed only in the ditch. The resultant CH₄ time series for the
493 chamber would have a characteristic appearance (Fig. S4) where the measurement would essentially start out as
494 diffusive flux measurement, then CH₄ bubbles entered the chamber headspace, and the concentration would
495 quickly increase to a maximum value and reach a threshold concentration corresponding to the mixed headspace
496 concentration. In these cases, the LM/HM flux calculation assumptions are violated and instead the ebullition
497 flux would be calculated as the total increase in CH₄ mass m⁻² per 5 min enclosure. The mass flux of CH₄ per
498 enclosure (nmol m⁻² per 5 min enclosure) was calculated according to Eq. (1):

499
$$F_{CH_4-ebu} = dCH_4 * \frac{V_{system}*P}{A*R*T} \quad (1)$$

500 Where dCH_4 is the concentration difference in nmol between start of chamber enclosure (CH_4_{start}) and end CH_4
 501 concentration (CH_4_{end}) after it reached a plateau (Fig. S4), V_{system} is the total volume (11.7 L) of the system
 502 (collar, chamber, tubes and GHG analyser) in L, P is the pressure (1 atm), A is the area of the collar (0.028 m²),
 503 R is the gas constant (0.082057 L atm K⁻¹ mol⁻¹) and T is the chamber headspace temperature (K). To calculate
 504 the ebullition flux per second the ebullition flux estimate was divided by 12*60 seconds (300), equivalent to the
 505 number of seconds over the 5 minute measurement period. The time step of dCH_4 was assumed to be 1 second
 506 meaning that the flux unit is nmol $CH_4 \cdot m^{-2} \cdot s^{-1}$.

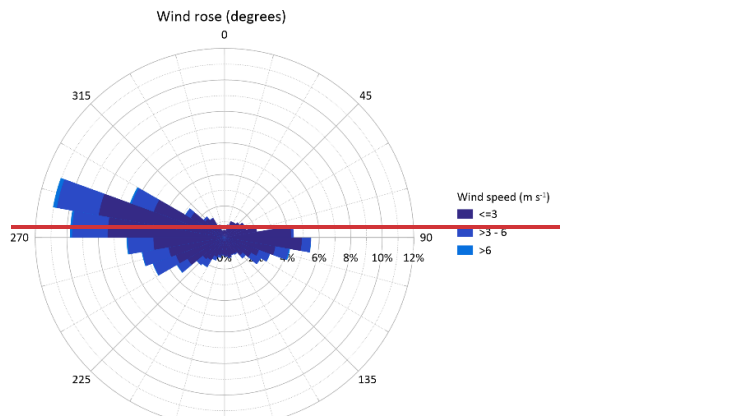
507 Out of a total of 1728 flux measurements from the ditch (collar 10), 334 were classified as ebullitions according
 508 to our definition above, indicating that ebullition was erratic which is in line with studies of ebullition of fluxes
 509 from ponds (Sø et al., 2023; Wik et al., 2016). Hence, it can be assumed that ebullition occurred around 19.3%
 510 of the time during the measurement period (360 days). An annual estimate of the ebullition flux was calculated
 511 as the average ebullition flux in nmol $CH_4 \cdot m^{-2} \cdot s^{-1}$ by multiplying with number of seconds over 365 days and the
 512 19.3% during period where ebullition occurred. Furthermore, the ebullition flux is calculated as the accumulated
 513 CH_4 in the chamber headspace during the entire flux measurement, e.g. 5 minutes here, and the calculated
 514 ebullition flux in the data set is therefore representative of 5 minute enclosure and not per second. To extrapolate
 515 to an annual estimate the number of 5 minute enclosures in 19% of 360 days is therefore estimated (N=20049.5-
 516 min 360 days⁻¹), multiplied with the average ebullition flux (nmol $CH_4 \cdot m^{-2} \cdot 5 \cdot min^{-1}$).

517 Ebullitions could also be caused by mechanical disturbance of the chamber landing on the collar. Ebullition
 518 fluxes were discarded if the sudden increase in CH_4 headspace concentration (Fig. S4) occurred 30-60 seconds
 519 after recorded chamber closure as this indicated bubbles released by chamber deployment on top of the collar.
 520

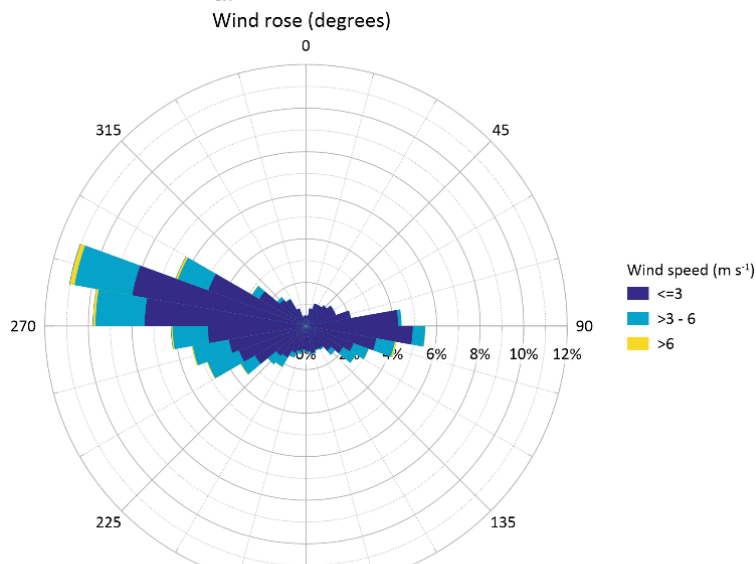
521 **3 Data presentation**

522 **3.1 Wind speed and direction**

523 Generally, the wind regime during the measurement period ([February 2nd, 2022 to January 28th, 2023](#)) was rather
524 mild with monthly average wind speeds ranging between 1.2 to 2.9 m s⁻¹ and maximum gust up to 20 m s⁻¹. The
525 wind direction was uniformly from the west for 52% of the time, with easterly winds constituting 27% and
526 northern and southern winds 8 and 13% of the time (Fig. 43). Winds from western directions were highest for
527 the longest period, while easterly winds were of similar magnitude, but less frequent (Fig. 43). Northern and
528 southerly winds were generally below 3 m s⁻¹ and represented periods with still conditions. The very uniform
529 western-eastern wind field at Vejrumbro may also partly be explained by the W-E direction of the valley in
530 which the site is situated, that effectively blocks or dampens winds from S and N.

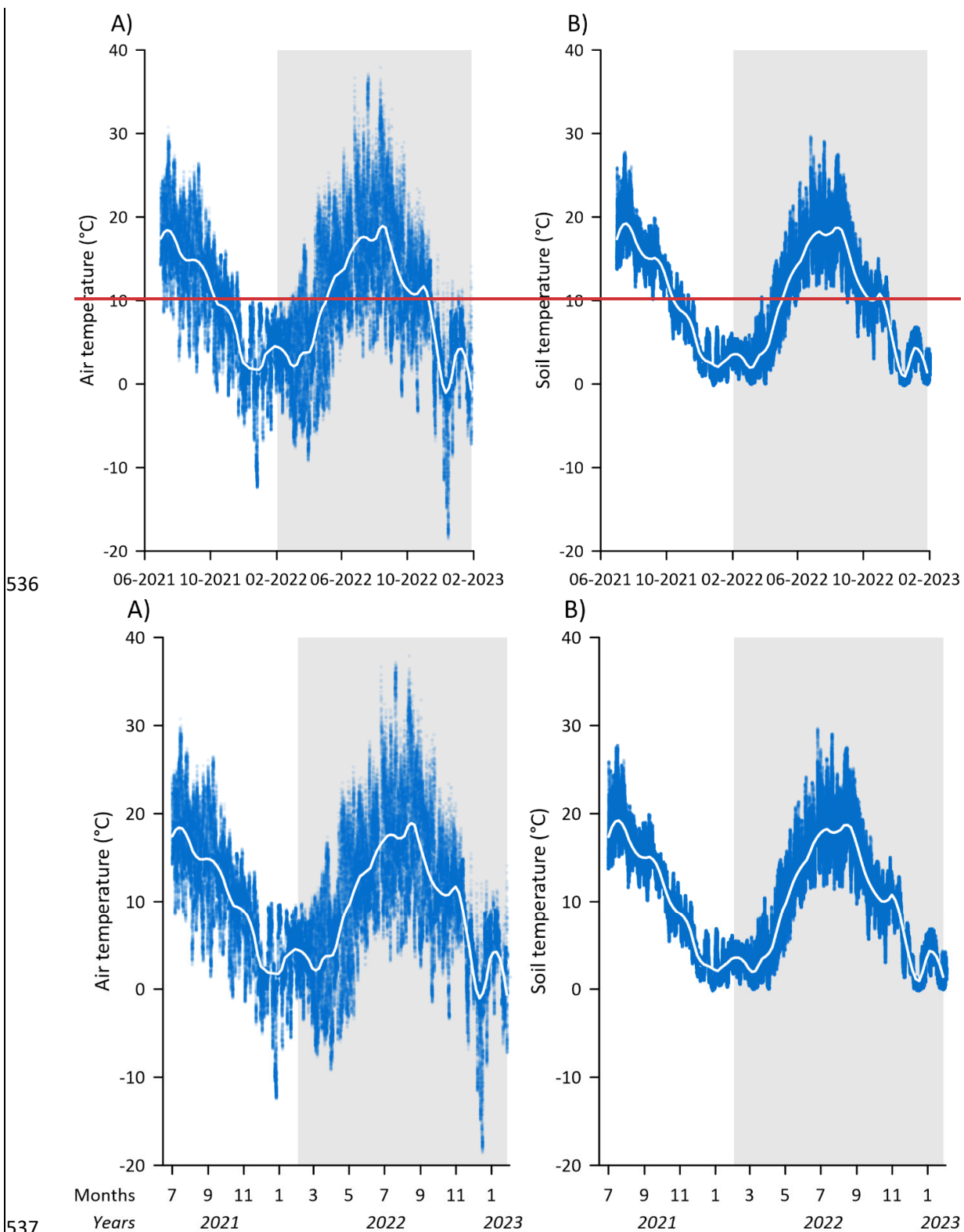


531



532

533 **Figure 34: Wind regime at Vejrumbro for the period July 1st, 2021 to January 31st, 2023 presented as a wind rose**
534 **diagram with wind speed and direction for the period.**



538 Figure 45: Time series of A) air temperature in $^{\circ}\text{C}$ measured at 2 meter height above the surface and B) soil
 539 temperature ($^{\circ}\text{C}$) at 5 cm depth for collars 4, 7, 9, 23 and 27 along the measurement transect. The blue dots are the

540 raw 5 min measurements of air temperature and the white lines represent LOESS fit to show overall seasonal trend.
541 The periods of GHG measurements with the SkyLine2D system are shown with the shaded area.

542 Over the study period the average air temperature was 9.6°C ranging between maximum 37.9°C and minimum
543 of -18.6°C (Fig. [5A4A](#)). Monthly ranges of air temperatures (Table 2) show >20°C variation between minimum
544 and maximum, except for February, pointing towards large diurnal variations. Soil temperature magnitude and
545 temporal variation were similar across the transect, varying between 0 to 28°C (Fig. [5B4B](#)) and followed that of
546 air temperature (Fig. [5A4A](#)) with less variability (Fig. [5B-4B](#) and Table [32](#)). The annual site average soil
547 temperature was similar to the air temperature (Table [32](#)).

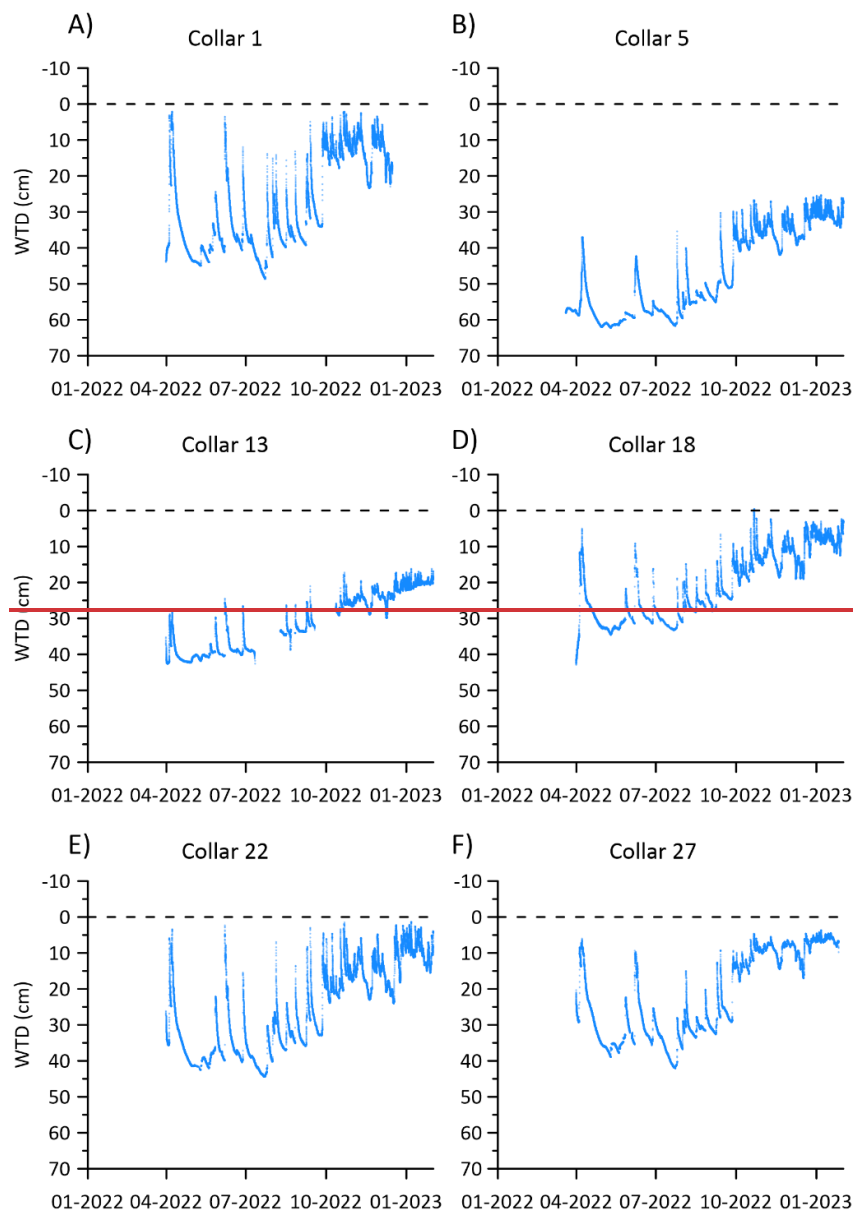
548 **Table 2: Monthly mean, maximum and minimum air temperature and soil temperature (°C), groundwater table**
 549 **depth (cm) and volumetric soil water content (cm³ cm⁻³) at Vejrumbro in the measurement period from February 1st,**
 550 **2022 to January 31st, 2023.**

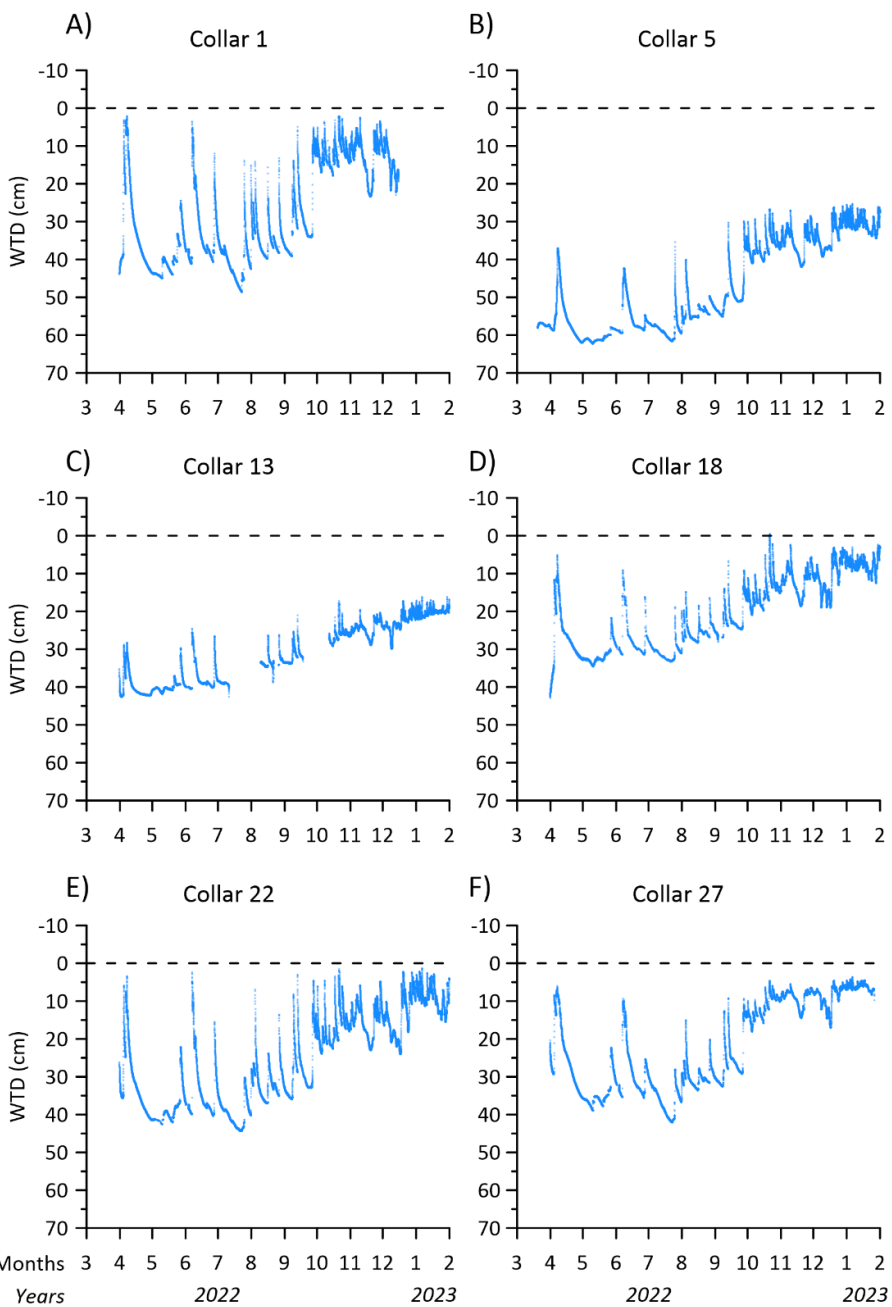
Variable	Month	2022										2023		
		Feb	Mar	Apr	May	Jun	Jul	Aug	Sep	Oct	Nov	Dec	Jan	Avg
Air temperature (°C)	Mean	3.8	3.0	6.6	12.0	15.4	17.7	16.6	13.4	10.7	6.9	1.2	3.7	9.6
	Max	10.6	17.4	23.7	25.3	36.7	37.2	37.9	32.9	23.3	18.4	12.4	14.1	-
	Min	-4.3	-9.3	-8.3	-3.4	4.3	3.2	2.7	-1.5	-3.5	-6.9	-18.6	-7.3	-
Soil temperature (°C)	Mean	3.0	3.2	2.9	6.4	12.3	16.1	18.4	17.0	13.8	10.3	7.2	2.1	9.6
	Max	6.5	5.3	9.1	12.5	18.8	25.1	27.0	24.7	19.3	14.3	12.6	6.3	-
	Min	0.3	1.1	0.4	0.8	6.6	10.7	12.4	11.8	7.0	4.0	2.1	0.0	-
Groundwater table depth (WTD) (cm)	Mean	-	39	35	41	36	41	35	31	20	18	17	13	29
	Max	-	58	39	58	43	52	46	36	30	31	28	28	-
	Min	-	23	5	24	9	28	22	9	5	6	3	2	-
Volumetric soil water content (cm ³ cm ⁻³)	Mean	0.53	0.45	0.40	0.37	0.38	0.43	0.43	0.45	0.50	0.53	0.52	0.51	0.46
	Max	0.56	0.51	0.50	0.41	0.47	0.55	0.56	0.56	0.57	0.58	0.56	0.57	-
	Min	0.43	0.39	0.37	0.33	0.32	0.26	0.32	0.35	0.40	0.47	0.42	0.34	-

551 **3.3 Groundwater table depth**

552 Average groundwater table depth (WTD) below terrain during the period was between 47 to 21 cm across the
 553 transect (Fig. 2, Table 23). During summer, the peat drained between 18 – 31 cm below the annual average and
 554 in winter the WTD increased to 0 – 22 cm above the annual average across the transect (Fig. 2, Table 23).

555 Generally, the WTD elevation was lower in the ditch across the entire study period (Fig. 2). It was only on the
 556 northern end of the transect that the surface occasionally was flooded during winter periods (Fig. 2).



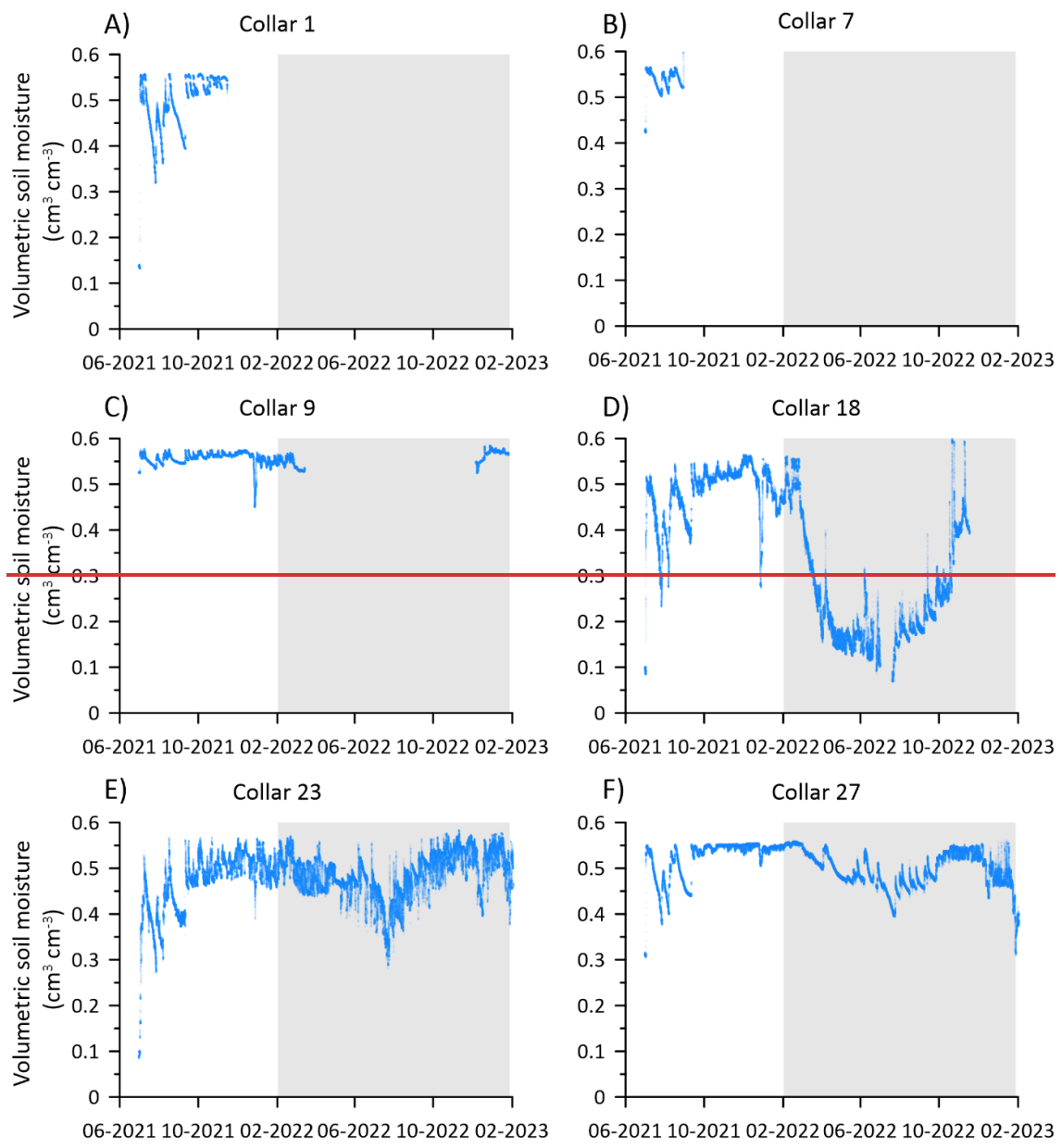


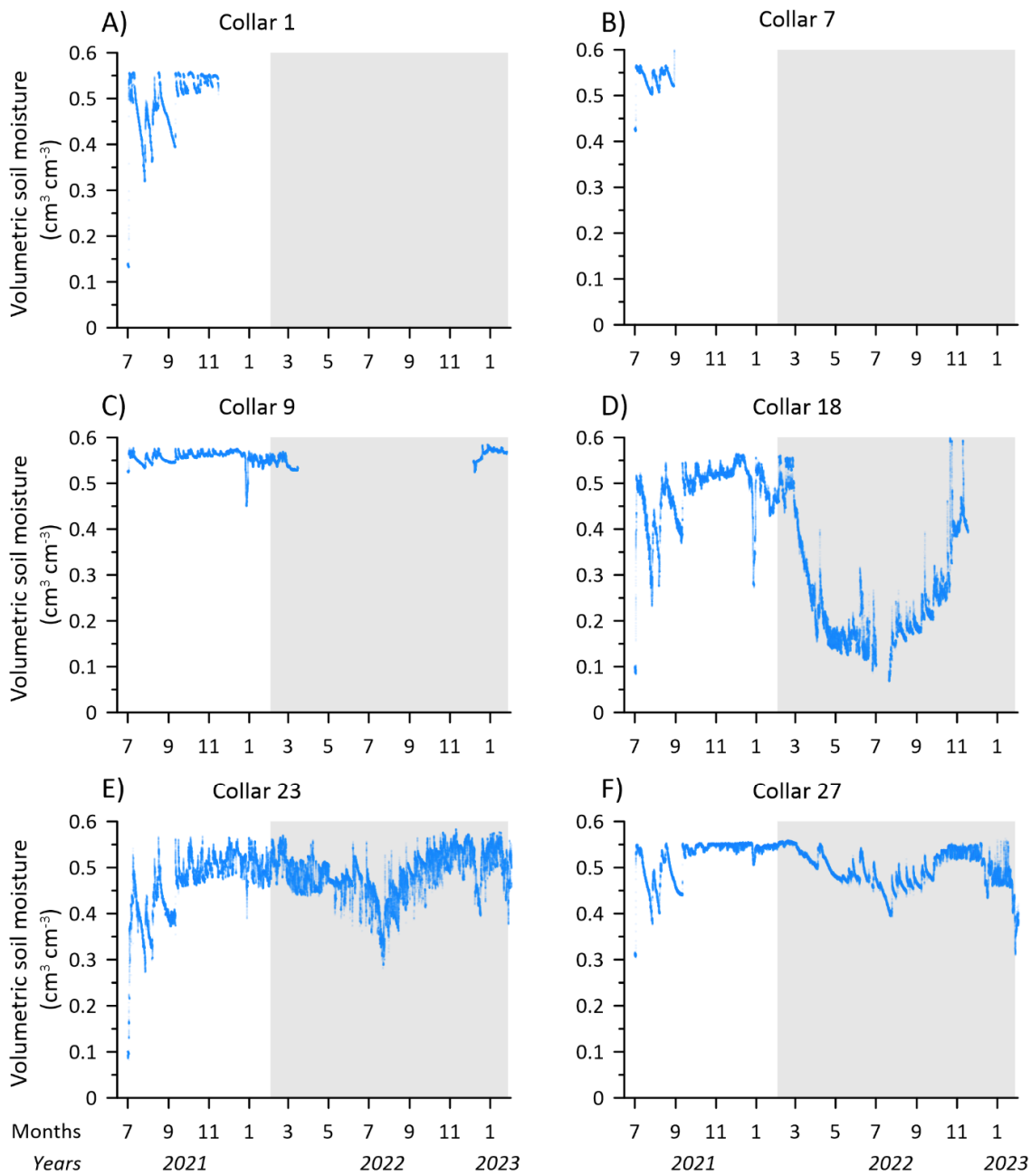
558
559 **Figure 56:** Time series of groundwater table depth (WTD) below terrain for the six piezometer locations along the
560 SkyLine2D transect in the period March 31st, 2022 and January 31st, 2023 when the flux measurements stopped.
561 Dashed line show surface.

562 The temporal variability of WTD was similar across the transect despite different absolute water table depths
563 (Fig. 65A-F). In the summer periods, the WTD was most variable decreasing to below -40 cm for collars 1, 13,
564 18, 22 and 27, whereas the WTD for collar 5 showed the deepest groundwater WTD measured ~~at over the~~
565 ~~transect the site~~. WTD responded quickly (within hours) to precipitation events that could increase the WTD by
566 almost 40 cm at some plots, indicating that the entire aerated soil volume above the groundwater table was
567 flooded. There was a slight tendency to lower response to precipitation events for piezometers at collar 5 and

568 collar 13 that were placed closer to the ditch (Fig. 2 and [Fig. 6B-5B](#) and C). As the ditch water level was lower
569 than in the peat this could be explained by more efficient lateral drainage into the ditch from the areas closer to
570 the ditch. In the winter periods, the WTD was less responsive to precipitation and was closer to the surface (Fig.
571 [56](#)A-F) across the transect.

572 **3.5 Soil water content**





574
575 **Figure 67:** Time series of volumetric soil water content ($\text{cm}^3 \text{cm}^{-3}$) in 0-5 cm for the six collars 1, 7, 9, 18, 23 and 27
576 along the SkyLine2D transect in the period July 1st, 2021 – January 31st, 2023 when the measurements terminated.
577 The periods of GHG measurements with the SkyLine2D system are shown (green lines) on the x-axis with the shaded
578 area.

579 Due to instrument failure the temporal coverage of soil moisture in the topsoil (5 cm) was not similar across the
580 transect (Fig. 76A-F). For collars 18, 23 and 27 the entire period of greenhouse gas measurements was covered
581 by soil moisture measurements (Fig. 76D-F). While SWC for collars 1, 9, 18, 23 and 27 was similar in the
582 winter periods (around $0.55 \text{ cm}^3 \text{cm}^{-3}$) the SWC for collar 18 decreased to lower minima between $0.1 – 0.2 \text{ cm}^3$
583 cm^{-3} , than the minima observed between $0.3 – 0.4 \text{ cm}^3 \text{cm}^{-3}$ for collars 23 and 27 in the summer periods (Fig. 76).

584 Table 23). Similar for all collars it was observed that SWC was more variable in summer, responding similarly
 585 as WTD to precipitation events (Fig. 76, Table 23). Since plants were removed regularly from the collars the
 586 decrease of SWC for collar 18 cannot be explained by plant transpiration, and the dynamic behaviour could
 587 indicate the impact of soil evaporation, but the different levels of SWC also show that there is spatial variation
 588 across the transect in the water retention drying properties of the peat soil that will impact the rate of drying.
 589 However, it cannot be ruled out that the SWC sensor at collar 18 experienced malfunction or that soil contact
 590 was lost in the dry periods of 2022 (Fig. 67D) which could lead to erroneous and too low SWC. Therefore, these
 591 data should be considered with care.

592 3.6 Peat soil characteristics

593 **Table 3 Mean (\pm standard error of the mean (SE)) peat/organic soil characteristics of humification degree (Von Post),**
 594 **pH (H₂O), dry bulk density (ρ_{dry}), total C (TC) concentration, total N concentration (TN) and the C/N ratio for collars**
 595 **1, 2, 5, 6, 8 and 13 - 27 at the Vejrumbro transect.**

Depth (cm)	N	Von post		pH (H ₂ O)		ρ_{dry} (g cm ⁻³)		TC (%)		TN (%)		C/N	
		Min	Max	Mean	\pm SE	Mean	\pm SE	Mean	\pm SE	Mean	\pm SE	Mean	\pm SE
0-20	20	7	10	4.2	0.08	0.31	0.02	26	1.1	1.6	0.06	16	0.4
20-40	20	5	10	4.6	0.06	0.20	0.01	43	1.3	1.8	0.04	24	0.7
40-60	11	3	8	4.9	0.10	0.15	0.01	48	1.8	1.9	0.05	25	1.1
60-80	11	3	6	5.3	0.09	0.11	0.01	47	1.8	1.9	0.05	24	0.6
80-100	10	1	8	5.4	0.09	0.10	0.02	44	2.1	1.9	0.05	24	0.6

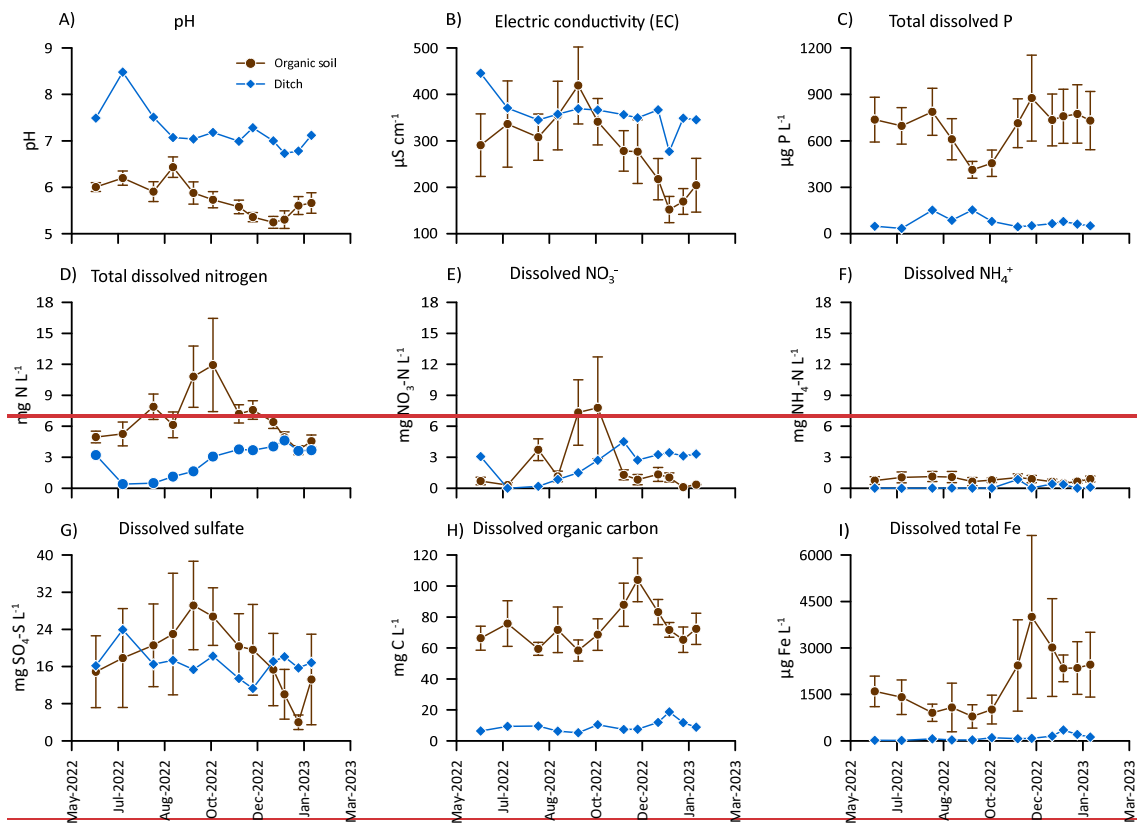
596 Generally, there was peat/organic soil to one meter depth except for one collar (25) where gytta was found in a
 597 depth of 80 cm (Table 3). The organic soil was more decomposed in the top 40 cm indicated by higher Von Post
 598 values between 5 and 10. Below 40 cm peat still displayed high levels of decomposition along the transect, but
 599 was more often found to be less decomposed, values ranging from 1-8 (Table 3). This corresponds well to the
 600 previous land use with drainage of the topsoil leading to higher degree of humification. Also, the organic soil
 601 was most dense in the top 20 cm (on average 0.31 ± 0.02 g cm⁻³) and bulk density decreased to $0.10 - 0.12$ g cm⁻³
 602 from 40 – 100 cm depth. Total C and N was lowest in the 0-20 cm layer, but still classified as organic soil.
 603 Below 20 cm total C and N concentrations, respectively were similar. C/N ratio was lowest in the top 20 cm
 604 (16 ± 0.4) and increased to 22-25 in 20 – 100 cm depth (Table 3).

605 3.6-7 Groundwater and ditch water chemical composition

606 Site mean pH of the groundwater in the organic soil was 5.8 ± 0.1 and was lower than the pH of the ditch
 607 (7.3 ± 0.6). There was a tendency towards lower pH in groundwater and ditch towards the end of the
 608 measurement period (Fig. 8A7A). Electric conductivity was generally higher in the ditch water (359 ± 36 μ S cm⁻¹)
 609 compared to the groundwater in the organic soil (276 ± 18 μ S cm⁻¹) but varied less over the season. The
 610 groundwater shows a clear peak in EC around September 2022 (Fig. 78B). Total dissolved P was markedly
 611 higher in the groundwater (687 ± 45 μ g P L⁻¹) compared to the ditch water (76 ± 10 μ g P L⁻¹). Whereas there was
 612 little seasonal trend in ditch P concentrations, dissolved P in groundwater dipped to below average
 613 concentrations between August to October, likely indicating plant uptake during the growing season (Fig. 78C).
 614 Similarly, total dissolved N was higher in groundwater (6.7 ± 0.5 mg N L⁻¹) than in ditch (2.6 ± 1.6 mg N L⁻¹) with
 615 increasing concentrations during the growing season (Fig. 78D). Similar, tThis temporal trend was also observed

616 for NO_3^- (Fig. 78E), but average groundwater ($2\pm0.5 \text{ mg NO}_3\text{-N L}^{-1}$) and ditch ($2.2\pm1.5 \text{ mg NO}_3\text{-N L}^{-1}$)
617 concentrations were similar. As expected, dissolved $\text{NH}_4\text{-N}$ was lowest among investigated N-species and there
618 was more dissolved $\text{NH}_4\text{-N}$ present in groundwater ($0.8\pm0.1 \text{ mg NH}_4\text{-N L}^{-1}$) than in the ditch ($0.14\pm0.25 \text{ mg}$
619 $\text{NH}_4\text{-N L}^{-1}$). However, there was no discernable temporal trend for NH_4^+ (Fig. 78F). Collectively, the temporal
620 trend of TN and NO_3^- could point to temperature driven mineralization of the peat. Also, the organic N (TN –
621 inorganic N-species) was on average 10 times higher in the groundwater than in the ditch. Average SO_4^{2-}
622 concentrations were similar between the groundwater ($17.5\pm2.4 \text{ mg SO}_4\text{-S L}^{-1}$) and ditch ($17\pm1.5 \text{ mg SO}_4\text{-S L}^{-1}$),
623 but SO_4^{2-} concentration peaked during September and October in the groundwater whereas it remained more
624 constant in the ditch over the season (Fig. 78G). Like the dissolved organic N, DOC concentrations were
625 consistently higher in the groundwater ($73\pm3.1 \text{ mg DOC L}^{-1}$) than in the ditch ($9.4\pm3.5 \text{ mg DOC L}^{-1}$), but
626 peaked later in the season, around December 2022, whereas there was little temporal variability of DOC in the
627 ditch (Fig. 78H). Dissolved total Fe displayed the same temporal trend as DOC (Fig. 78I) but was higher
628 groundwater ($1916\pm163 \mu\text{g Fe L}^{-1}$) compared to the ditch ($98\pm95 \mu\text{g Fe L}^{-1}$). The geochemical parameters of
629 groundwater and ditch water point to different mechanisms regulating ~~especially elements related to~~ peat
630 decomposition and possibly plant uptake, where the chemical composition of groundwater varied more over
631 time was more dynamic over time than ditch water. Generally, there were no systematic spatial pattern of
632 groundwater chemistry across the transect.

633



634

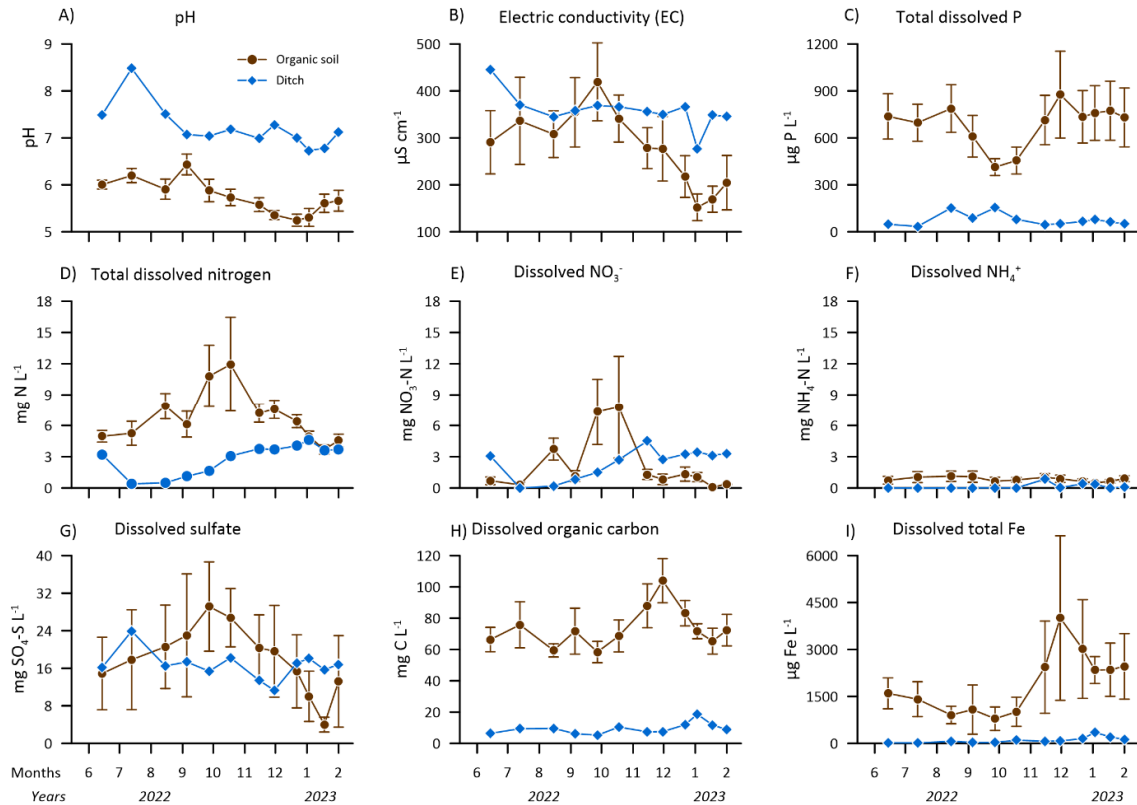
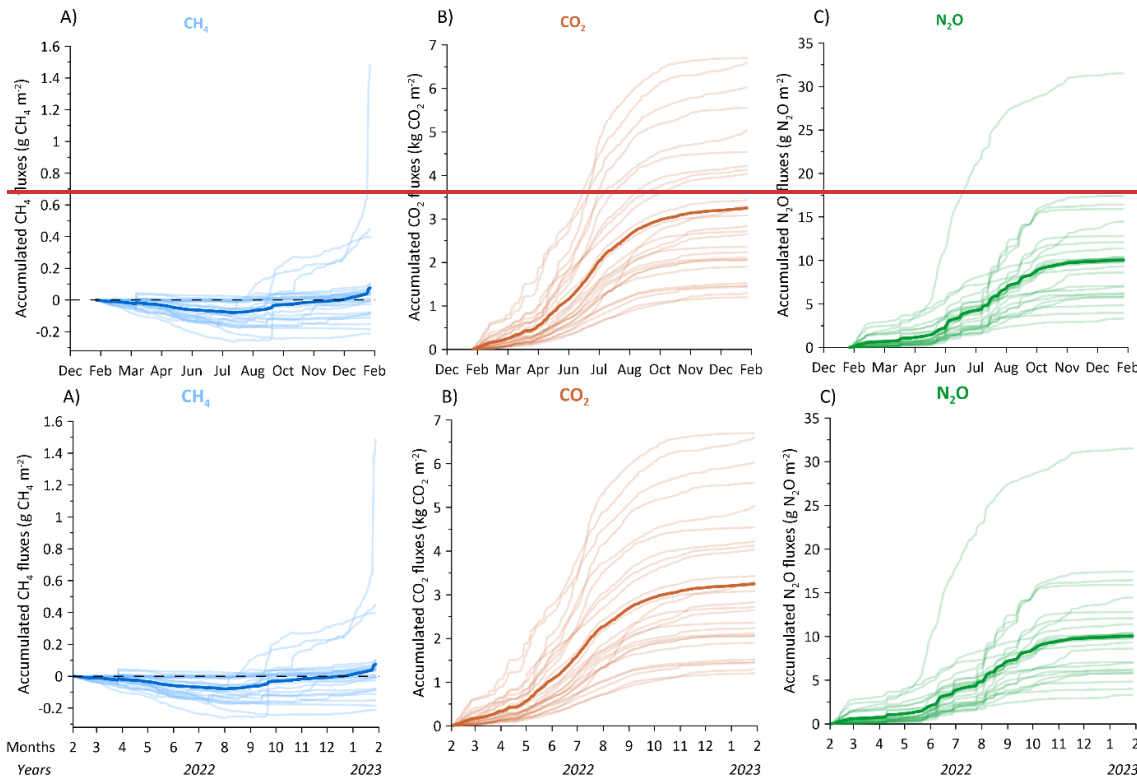
635
636

Figure 7 Groundwater (brown closed circles) and ditch water (closed blue diamonds) chemistry at Vejrumbro for the period June 2022 to February 2023 for A) pH, B) Electric conductivity and dissolved C) total phosphor (P), D) total

637 nitrogen (N), E) nitrate (NO_3^-), F) ammonium (NH_4^+), G) sulfate (SO_4^{2-}), H) organic carbon and I) total iron (Fe).
 638 Values for organic soils are site-means for the transect with error bars showing the standard error of the mean (N=6
 639 per sampling date).

640 **3.7-8 Net soil and ditch CO_2 , CH_4 and N_2O fluxes**

641 **3.7-8.1 Spatial variation of net soil CO_2 , CH_4 and N_2O fluxes**



642
 643 **Figure 89: Cumulative fluxes of A) CH_4 , B) CO_2 , and C) N_2O for 26 individual collars along the SkyLine2D transect
 644 in the measurement period February 2022 to January 2023. Units for CH_4 and N_2O are in $\text{g CH}_4/\text{N}_2\text{O m}^{-2}$ and for
 645 CO_2 in $\text{kg CO}_2 \text{m}^{-2}$. The cumulative fluxes represent the raw dataset. The ditch data was excluded. Site-Transect
 646 average is shown as thick lines.**

647 Within the transect, cumulative CH_4 fluxes over the study period (360 days) varied between -0.21 to 1.48 $\text{g CH}_4 \text{m}^{-2}$ over the study period, with a site-transect average ($\pm \text{SE}$) cumulative flux of $0.07 \pm 0.06 \text{ g CH}_4 \text{m}^{-2}$ (Fig. 2 and Fig. 9A8A). Out of the 26 collars, excluding the ditch collar, 11 displayed a net uptake over the measurement period and the remaining were small net emitters (Fig. 2 and Fig. 9A8A). There was generally little spatial variation in the absolute CH_4 fluxes among the soil collars, but three collars (11, 12 and 15) showed increasing net positive cumulative fluxes towards the ditch (Fig. 2). The low spatial and similar temporal variation between collars indicate both hydrological indicators of SWC and WTD are poor predictors of CH_4 fluxes across the this site transect. However, as we excluded plants from the collars we might have decreased the net emission of CH_4 directly by restricting gas transport in aerenchyma from deep peat layers potentially sustaining net CH_4 emission even though the observed growing season WTD was 20-40 cm (Askaer et al., 2011; Vroom et al., 2022) and indirectly by potentially reducing plant carbon supply to methanogens. (Bridgeman et al. 2013), limiting net CH_4 emission However, visible inspection at the site confirmed lateral root growth from vegetation adjacent to the

660 collar. This could indicate that plant derived C and N was still available for microbes underneath the collars, but
661 the impact on gas transport is uncertain. However, we did not excavate roots during the study to avoid excessive
662 disturbance. Furthermore, considering that the WTD in the growing season was mostly 20–40 cm below terrain
663 the potential for CH₄ production in the topsoil would be limited. Also, the lack of consistent hot moments of CH₄
664 emissions, and low cumulative emissions during periods of shallow WTD in the growing season (Fig. 5A–F) is
665 in line with the measured from the soil despite hydrological conditions in the subsoil being conducive for CH₄
666 production could indicate that redox potential is elevated due to presence of other electron acceptors. The
667 presence of both free NO₃[−], SO₄^{2−}, Fe ions (Fig. 8E, G, I) in the groundwater. It is well known that the presence
668 of other electron acceptors, such as sulphur, iron and nitrate, inhibit CH₄ production (Bridgman et al., 2013), in
669 turn limiting net CH₄ emission. Also, the often deeper WTD in the summer between 20–40 cm below terrain
670 also suggest that CH₄ oxidation could aid to reduce net CH₄ emission from the peat in the groundwater could
671 indicate that there are alternative electron acceptors that prevent lowering of the redox status of the soil and
672 hence suppresses CH₄ production (Christiansen et al., 2016).

673 The CO₂ effluxes displayed tremendous spatial variation across the 24-meter transect (Fig. 2 and Fig. 9B8B)
674 and measurements indicated that the drained organic soil was a net source of CO₂, with cumulative fluxes over
675 the study period ranging between 1214–6740 g CO₂ m^{−2}, and a site transect average (±SE) of 3269±328 g CO₂
676 m^{−2}, over the study period of 360 days (Fig. 2 and Fig. 9B8B). There was no apparent relation between the
677 magnitude of cumulative CO₂ efflux to the position along the transect and average WTD (Fig. 2). The
678 cumulative net soil CO₂ emission is equal to 8.9 tCO₂-C ha^{−1} y^{−1} (range of 3.3 to 18 tCO₂-C ha^{−1} y^{−1} across the
679 transect) and compares well to estimates of annual soil C loss (8.8 tCO₂-C ha^{−1} y^{−1}) from a drained unfertilized
680 grassland on organic soil in Denmark (Kandel et al., 2018) as well as annual carbon budgets of similar Danish,
681 British and German wetlands (Evans et al., 2021; Koch et al., 2023; Tiemeyer et al., 2020).

682 Similarly, the particular site at Vejrumbro where the SkyLine2D was located was overall a net source of N₂O,
683 with cumulative fluxes ranging between 3.3–32 g N₂O m^{−2}, with a site transect average (±SE) of 10.1±1.1 g
684 N₂O m^{−2} (Fig. 2 and Fig. 98C) over the study period (360 days). Thus, there is a 10-fold difference between
685 minimum and maximum cumulative N₂O fluxes within the transect, without any apparent relation to the
686 position along the transect and WTD. The highest cumulative N₂O fluxes occurred at collar 8 situated close to
687 the ditch (Fig. 2). The site transect average cumulative N₂O emission is equivalent to a net N loss from N₂O
688 emission alone of 64 kg N ha^{−1} y^{−1}, was very high and exceeding previously reported fluxes from the this
689 site Vejrumbro site (1.5–2.1 g N₂O m^{−2} y^{−1}) (Nielsen et al., 2024) and German organic soils (0.04–6.3 g N₂O
690 m^{−2} y^{−1} for grassland and cropland land uses) (Tiemeyer et al., 2020). The high N₂O emission from this the site
691 transect during the measurement period indicate that N₂O may in fact dominate the GWP GHG budget in
692 relation to the global warming potential at this specific location at the Vejrumbro site had gross primary
693 production (reducing net ecosystem CO₂ emission) been included in the measurements. It is important to
694 reiterate here that the flux measurements of this study were done on bare soil whereas the studies referenced
695 above included vegetation.

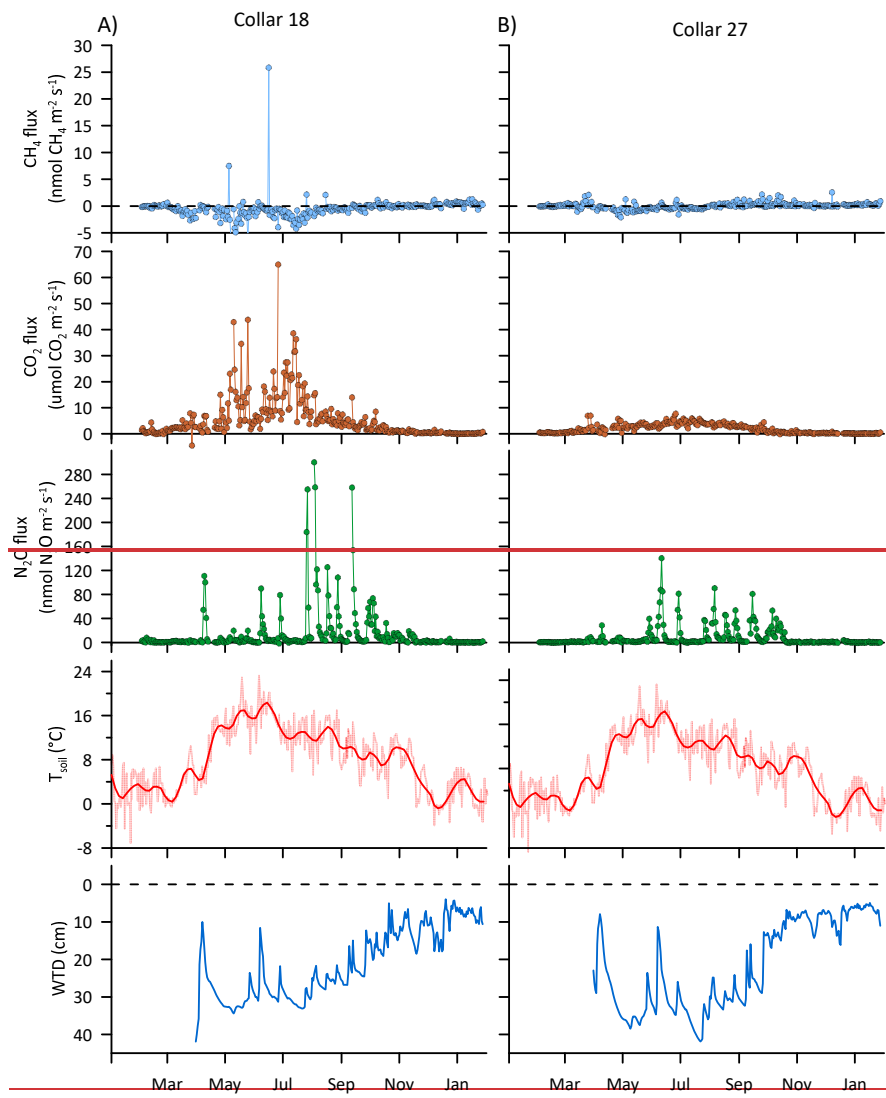
696 The high N₂O fluxes may be a result of high rates of denitrification in the subsoil from either *in situ* produced
697 NO₃[−] from peat decomposition or as NO₃-enriched agricultural runoff from the surrounding intensively
698 cultivated areas, which was not affecting groundwater NO₃[−] concentration in the center of the wetland with

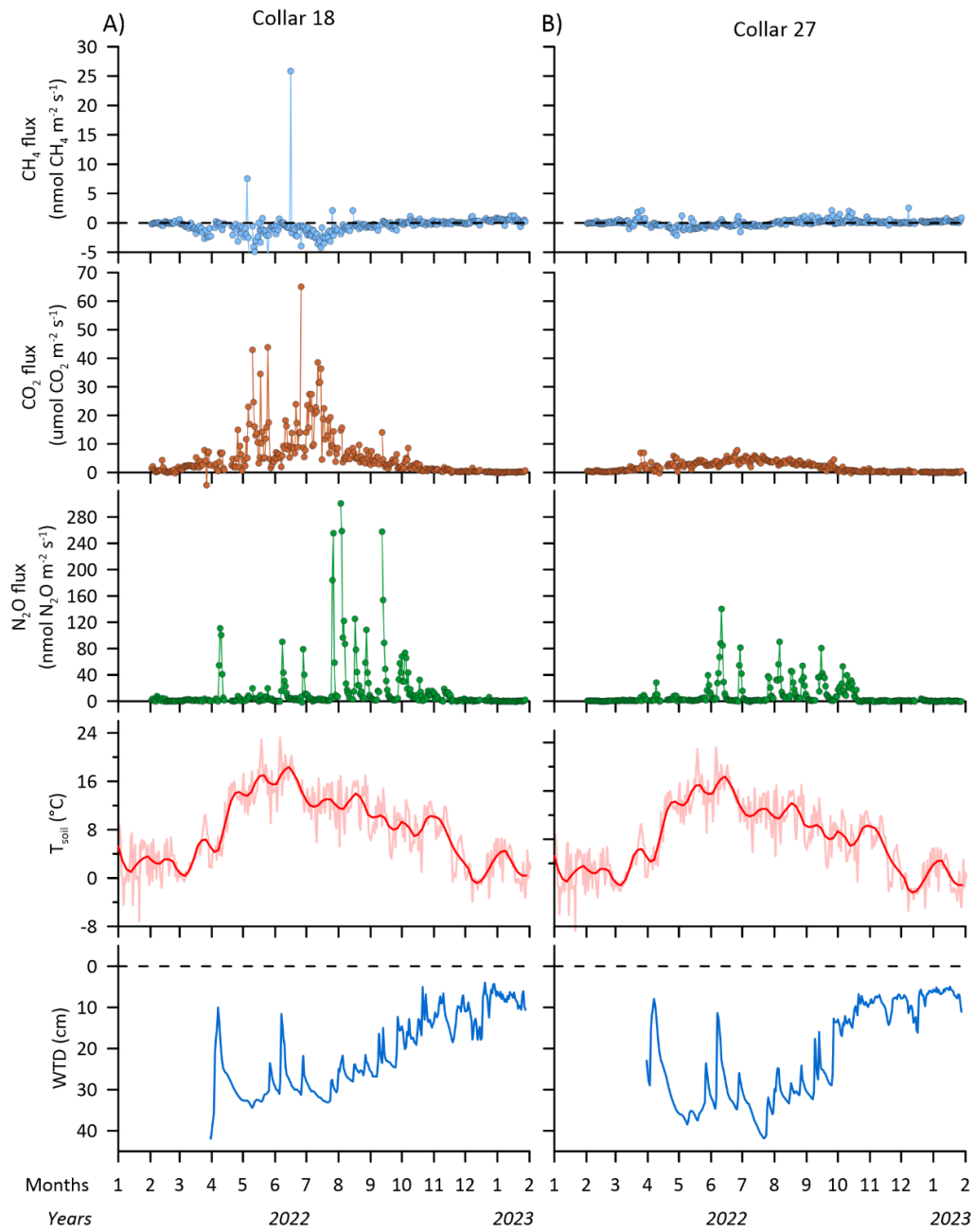
699 lower N₂O (Nielsen et al., 2024). The groundwater enters the northern peripheral zone of the wetland at
700 Vejrumbro coinciding with the position of the measurement transect. The highest NO₃⁻ concentrations in
701 groundwater at the SkyLine2D transect corresponded roughly with highest N₂O emissions~~S~~ during summer and
702 early autumn (Fig. ~~78~~D-F and Fig. ~~42~~D~~8~~C), but the frequency of water sampling was too low to fully link
703 groundwater NO₃⁻ temporal dynamics to N₂O emissions.

704

705 3.78.2 Temporal variability of net soil CO₂, CH₄ and N₂O fluxes

706 3.78.2.1 Time series of raw data of net soil CO₂, CH₄ and N₂O fluxes





708
 709 **Figure 9:** Examples of daily average time series of CH_4 , CO_2 and N_2O fluxes for collars 18 and 27 at the SkyLine2D
 710 transect in Vejrumbro, soil temperature (T_{soil}) in celsius ($^{\circ}\text{C}$) and groundwater table depth (WTD) in cm below
 711 terrain is shown in two lower panels for the measurement period from February 2022 to January 2023.

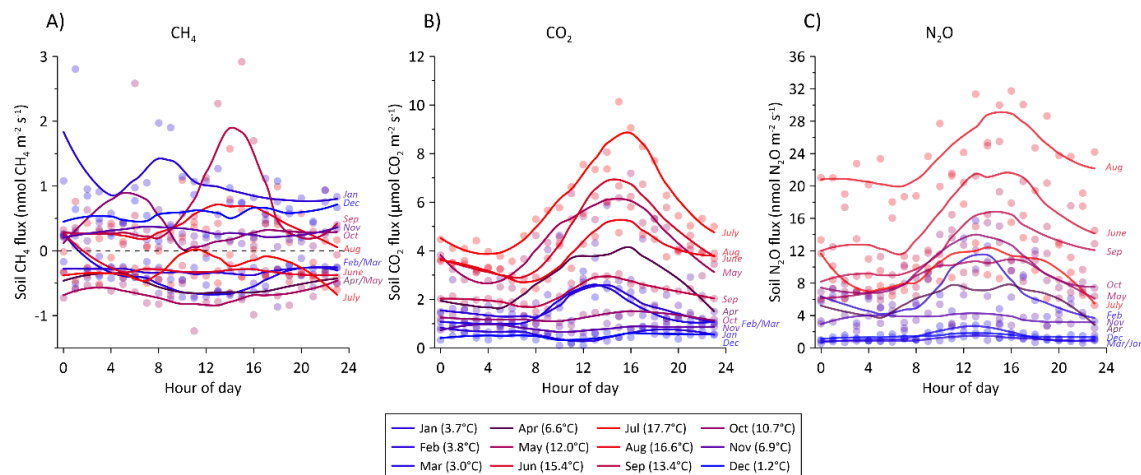
712 With the high frequency of GHG flux measurements (on average 5 measurements per day per collar) it was
 713 possible to observe short term flux phenomena that in most studies deploying manual chambers are missed or if
 714 captured can lead to biased conclusions on flux magnitudes. For example, in most of the measurement points,
 715 CH_4 fluxes were generally near zero, but occasionally displayed elevated net emission for short periods even in
 716 periods with deeper WTD (Fig. 10A9A) for most chambers (see supplementary Fig. S5). This flux dynamic
 717 might be related to episodic release of accumulated CH_4 from deeper soil layers that are not fully oxidized in the

718 aerated root zone and that were not released through plants (Askaer et al., 2011). As plants were not included in
719 the collars these bursts cannot be attributed to plant emission pathways.

720 Generally, it was observed that soil CO₂ fluxes increased over the season with increasing temperature. However,
721 for some collars displayed rapid bursts of CO₂ emissions (example in Fig. 10A9A), while other collars at the
722 same period did not display this behaviour (Fig. 10B9B). This dynamic points to different emission pathways
723 from the soil not related to plant mediated transport. Thus, while we purposely omitted aboveground autotrophic
724 respiration by clipping the vegetation, it cannot be ruled out that living roots inhabited the soil below the
725 chambers and hence contributed to the observed CO₂ emission rates.

726 For N₂O, the spatiotemporal pattern was even more pronounced than for CO₂, with N₂O primarily emitted in
727 bursts related to rapidly increasing or decreasing WTD that coincided with precipitation events. In drier periods
728 with deeper WTD and little fluctuations, N₂O fluxes quickly dropped to near zero (Fig. 10A-9A and B). Despite
729 N₂O being emitted in similar temporal patterns across the site transect, the magnitude of the N₂O peaks were not
730 similar across the transect (Fig. 2, 8 and supplementary Fig. S5). Hence, the majority of N₂O is emitted in hot
731 moments is likely driven by fluctuations in WTD mainly (Fig. 109) as it has also been shown in other drained
732 temperate peatland soils (Anthony and Silver, 2023).

733 3.78.2.2 Diurnal variation of net soil CO₂, CH₄ and N₂O fluxes

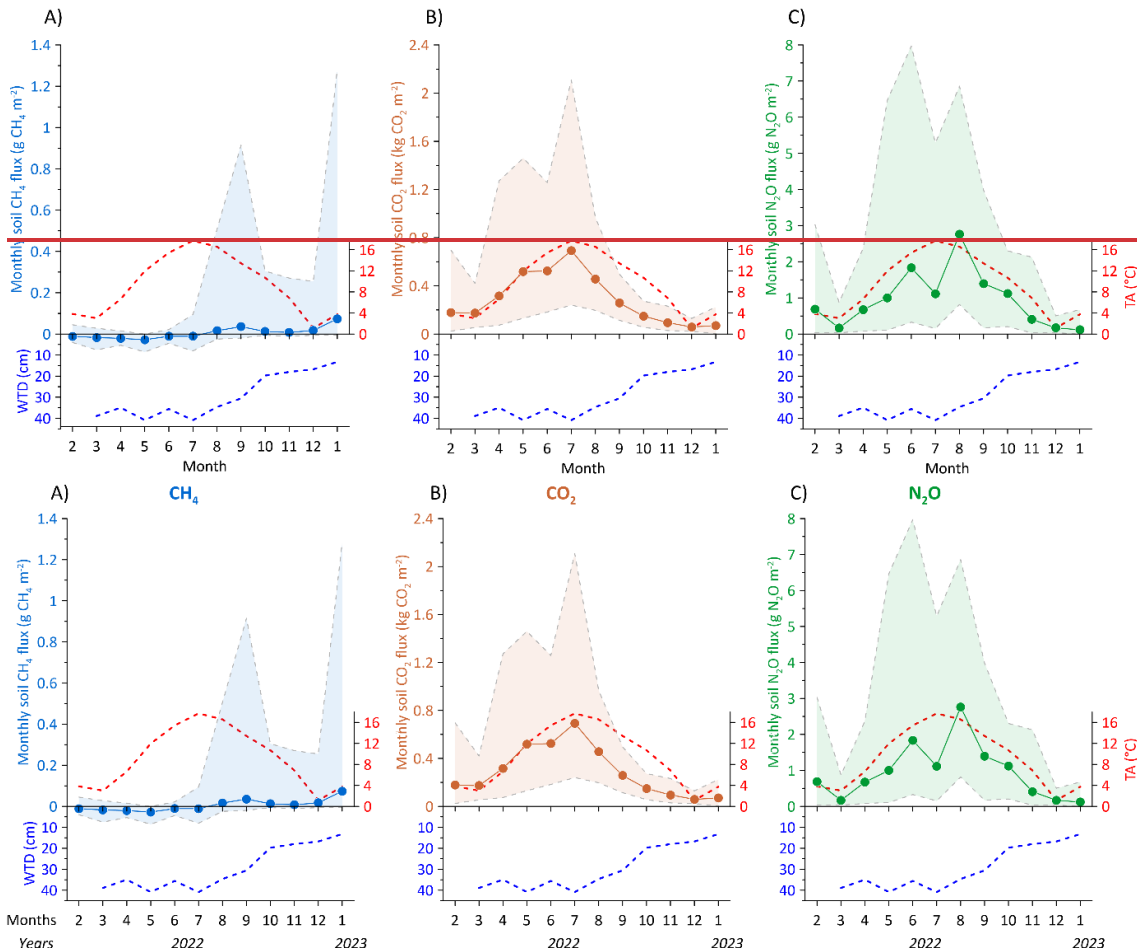


735 **Figure 1011:** Average hourly flux for all soil collars of A) CH₄, B) CO₂, and C) N₂O during a 24 hour period. The
736 diurnal variation is split between each month during the 2022-2023 measurement period. The fluxes were assigned
737 the hour of measurement during the day and averaged per month. Color shade between blue and red corresponds to
738 average air temperature for the specific month shown in parenthesis in the figure legend. Solid lines are loess fits for
739 visualization of the diurnal variation in each month.

740 With the SkyLine2D system we observed a clear diurnal cycle for CO₂ and N₂O fluxes, but not for CH₄ (Fig.
741 11A10A-C). The lack of diurnal variability of CH₄ fluxes could also be due the removal of plants from the
742 collars that would have facilitated light-driven fluxes (Askaer et al. 2011). The amplitude of diurnal variability
743 increased with higher air temperature for CO₂ (Fig. 11B10B) and partly for N₂O (Fig. 11C10C). The month of
744 July was an exception as it resembled the pattern observed in May although the July soil temperature was about
745 5°C higher (Table 22). The lower N₂O fluxes observed in July can be attributed to lower and more constant

746 WTD in July compared to May, June and September across the transect (Fig. 56). Diurnal variability of soil CO₂
 747 fluxes are well known and can be related to both increased heterotrophic respiration during the warmer day and
 748 autotrophic respiration in response to photosynthesis. Previously, similar diurnal patterns of N₂O emissions were
 749 observed in a Danish fen (Jørgensen et al., 2012).

750 **3.78.2.3 Monthly variability of net soil GHG fluxes**



751 **Figure 1142:** Monthly summed soil fluxes of A) CH₄ in g CH₄ m⁻², B) CO₂ in kg CO₂ m⁻², and C) N₂O in g N₂O m⁻² for
 752 all organic soil collars for the measurement period from February 2022 to January 2023. Shaded areas for CH₄, CO₂
 753 and N₂O graphs represent the maximum and minimum monthly average fluxes. Blue dashed line below CH₄, CO₂
 754 and N₂O represent the measured monthly average transect groundwater table depth (WTD) in cm below terrain. Red
 755 dashed line shows the monthly average air temperature (TA).
 756

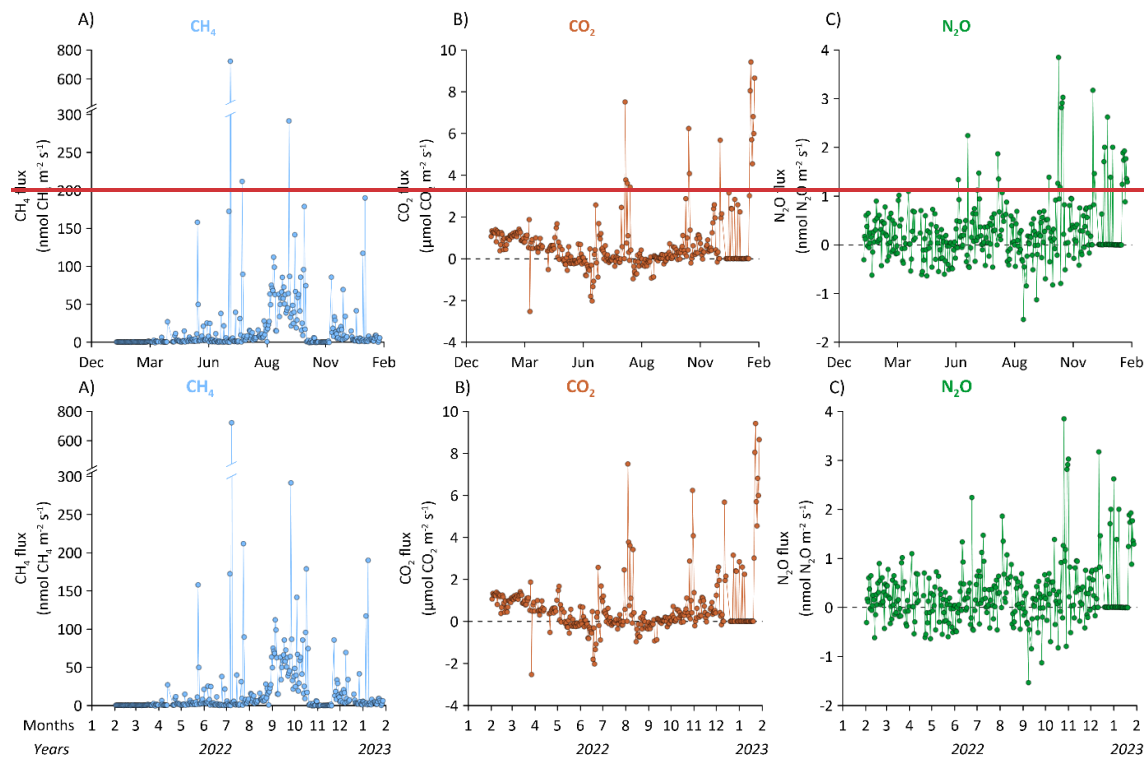
757 The average soil GHG fluxes for all collars were summed to monthly site-transect sums to illustrate long term
 758 drivers on the flux magnitude. Overall, monthly sums of CO₂ and N₂O emissions increase with temperature and
 759 fluxes are highest under deeper WTD, but CH₄ net fluxes were less responsive to long term changes in both
 760 temperature and hydrology (Fig. 12A-11A-C). Net uptake of CH₄ increased slightly with increasing temperature
 761 and lower WTD during the spring and summer. With increasing water table and high temperatures in August the
 762 soils across the site-transect turned into a small net CH₄ source continuing in fall and winter (Fig. 12A-11A).
 763

764 For CO₂ the seasonal variation was pronounced and closely followed soil temperature until peak values in July
 765 for both site transect average, minimum and maximum fluxes, respectively (Fig. 42B11B). From July to August,
 766 it was observed that WTD across the transect the site began to increase again and CO₂ fluxes departed from the
 767 close relation to soil temperature, indicating an inhibitory role of the WTD in this period, but reaching minimum
 768 fluxes in December, corresponding to the wettest and coldest month (Fig. 42B11B).

769 Similarly, N₂O fluxes increased with soil temperature reaching peak monthly values in August, corresponding to
 770 the period of the year with highest soil temperature and increasing WTD (Fig. 42C11C). This supports the
 771 promoting role of soil water saturation on the production of N₂O when temperature is favourable for
 772 denitrification. N₂O fluxes reached minimum values in December when WTD and ST were lowest (Fig.
 773 42C11C).

774 3.78.3 Ditch CO₂, CH₄ and N₂O fluxes

775 3.78.3.1 Time series of raw data of ditch CO₂, CH₄ and N₂O fluxes



776
 777
 778 **Figure 12.13:** Daily average time series of net ditch total A) CH₄ (diffusion and ebullition), B) CO₂, and C) N₂O fluxes
 779 at the Vejrumbro site for the measurement period from February 2022 to January 2023.

780 Common for all three gases is that ditch emissions are dynamic and net fluxes change from zero to large net
 781 positive or negative fluxes within hours or days (Fig. 13A12A-C). Compared to net soil CH₄ fluxes the ditch can
 782 be considered an emission hotspot at the Vejrumbro site (sum of diffusive diffusion and ebullition: 8.3 g CH₄ m⁻² y⁻¹), but fluxes are lower than earlier reports for ditches in other drained wetlands (between 0.1 – 44.3 g CH₄
 783 m⁻² y⁻¹) (Peacock et al., 2021). Methane varies most throughout the measurement period is most dynamic with
 784 maximum diffusive flux close to 700 nmol CH₄ m⁻² s⁻¹ and there was a tendency toward consistently higher net
 785

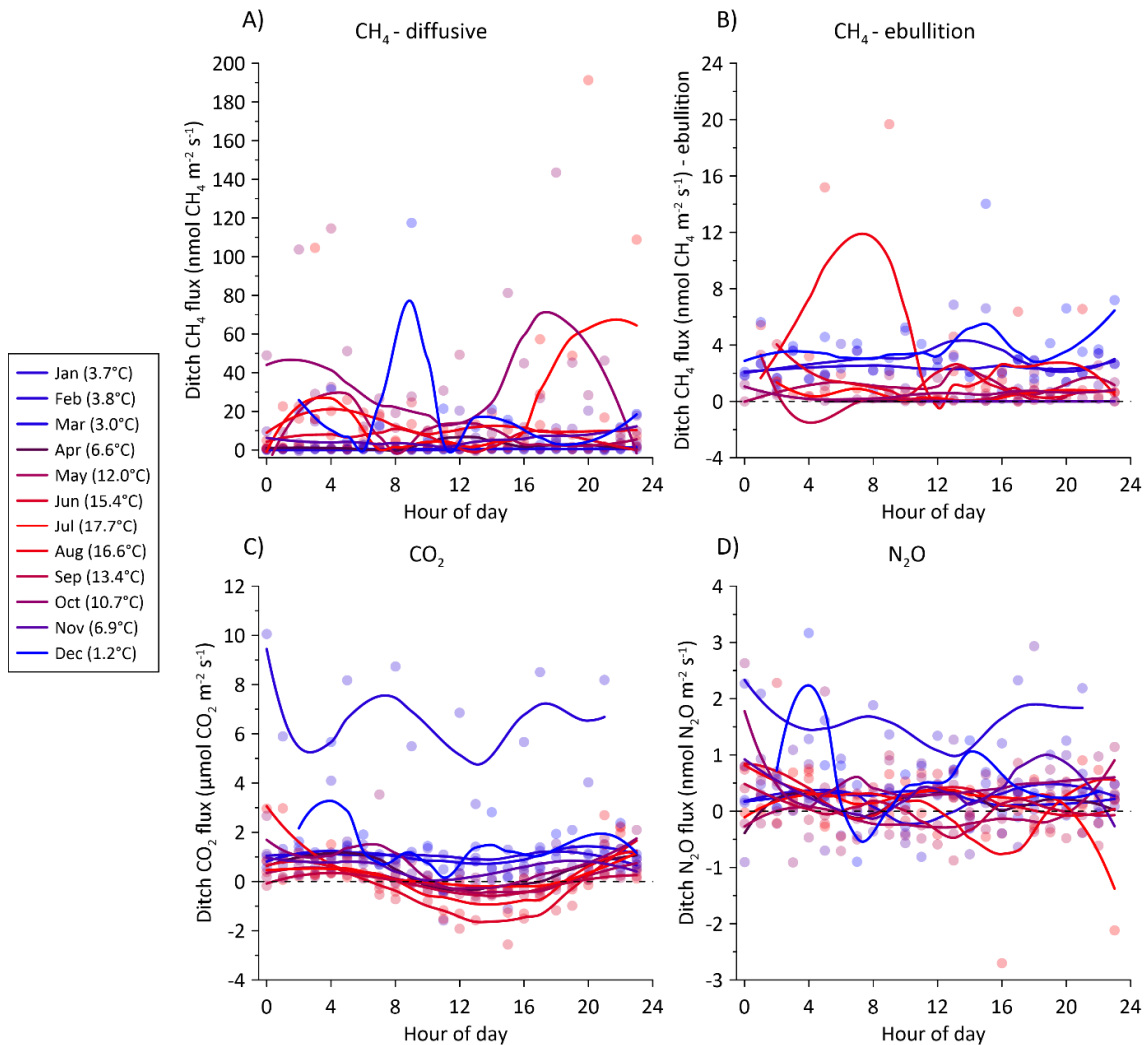
786 CH₄ emission from August to September, becoming close to zero in colder seasons (Fig. 13A12A). Ebullition of
787 CH₄ did occur occasionally in the ditch, e.g. about 19.3% of flux measurements for the ditch was comprised of
788 ebullitions but constituted on average only 2.9% of the total CH₄ emission (0.24 g CH₄ m⁻² y⁻¹) from the ditch
789 which is lower, but in the same range as a recent estimate from a ditch in a similar drained German peatland
790 (Köhn et al., 2021). According to the flux calculation methodology, flux separation and extrapolation to daily
791 sums, diffusive fluxes dominated (6.56 g CH₄ m⁻² y⁻¹). However, it cannot be ruled out that the classification as
792 diffusive flux may in fact be ebullition by nature. It has been suggested that microbubbles resulting from mass
793 transport can resemble diffusive fluxes in a chamber making it difficult, if not impossible, to fully separate the
794 two emission mechanisms in a continuous time series if headspace CH₄ concentrations do not abruptly increase
795 (Prairie and del Giorgio, 2013), such as in the example shown in Fig. S4.

796 For CO₂, there was a general tendency towards lower fluxes during the summer months and fluxes increased in
797 magnitude and variability towards the end of the study period (Fig. 13B12B). For N₂O, the fluxes fluctuated
798 around zero for most of the study period, except towards the end (December and January) where net fluxes
799 became positive (Fig. 13C12C).

800 Compared to the net soil N₂O and CO₂ fluxes the ditch fluxes of these gases are low showing that the ditch is
801 not contributing significantly to the CO₂ and N₂O budget at [this-the Vejrumbro](#) site.

802 Per square meter, the ditch emitted less N₂O (0.41 g N₂O m⁻² or 2.6 kg N₂O-N ha⁻¹ y⁻¹) and CO₂ (961 g CO₂ m⁻²
803 y⁻¹ or 2.6 tCO₂-C ha⁻¹ y⁻¹) than the organic soil, but was a hotspot of CH₄ emission (8.4 g CH₄ m⁻² y⁻¹ or 63 kg
804 CH₄-C ha⁻¹ y⁻¹) during the measurement period. Although these emissions estimates are lower than previously
805 reported for ditches in organic soil (up to 44 g CH₄ m⁻² y⁻¹) (Peacock et al., 2021). For the ditch CH₄ budget,
806 ebullition only constitutes 2.9% of net CH₄ emissions during the study period. This proportion may be
807 underestimated as the count of ebullition events may have been underestimated (Prairie and del Giorgio, 2013).

808 **3.78.3.2 Diurnal variability in ditch fluxes**



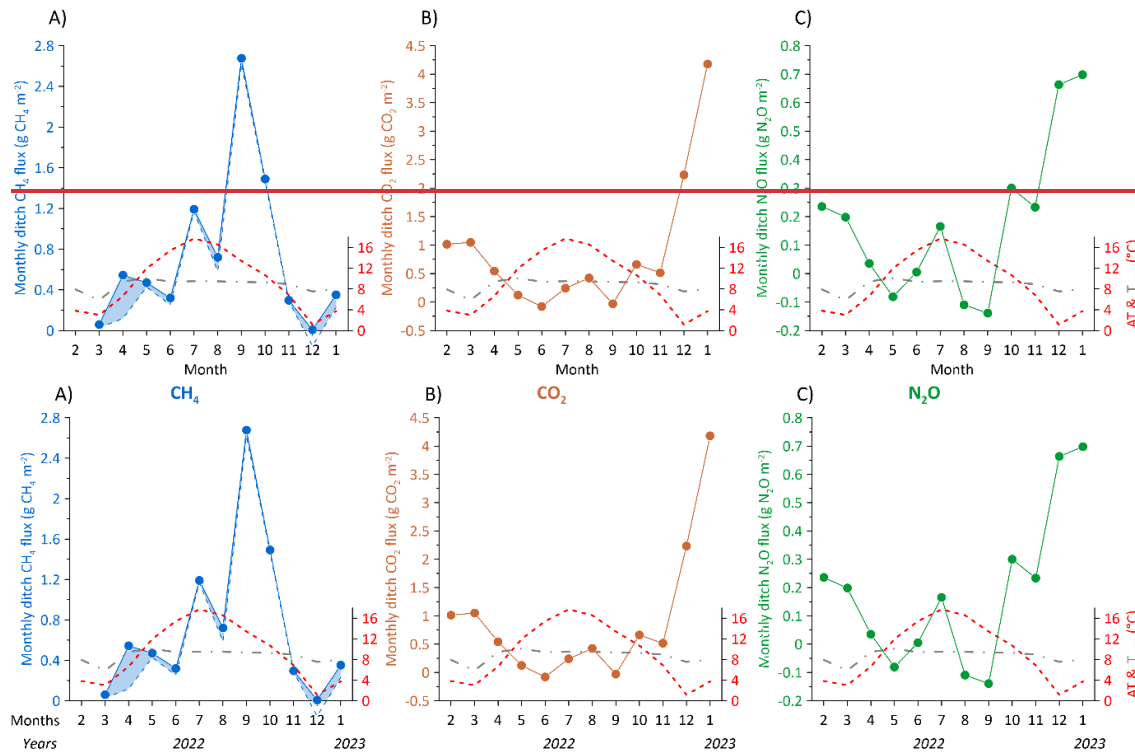
809

810 **Figure 13****4**: Average hourly fluxes for the ditch collar of A) diffusive CH₄ fluxes, B) CH₄ ebullition fluxes, C) CO₂,
 811 and C) N₂O during a 24 hour period. The fluxes were assigned the hour of measurement during the day and averaged
 812 per month. The diurnal variation is split between each month during the 2022-2023 measurement period. Color
 813 shade between blue and red corresponds to average air temperature for the specific month shown in parenthesis in
 814 the figure legend. Solid lines are loess fits for visualization of the diurnal variation in each month. Note different axes.

815 For CH₄ fluxes, both diffusive diffusion and ebullition, there was no clear diurnal variability in any month (Fig.
 816 14A-13A and B). This is expected for ebullition emissions which is known to be erratic without any clear
 817 diurnality (Sø et al., 2023; Wik et al., 2016). For net CO₂ fluxes from the ditch there was no diurnal variability
 818 in colder seasons (Jan, Feb, Mar, Nov and Dec), but consistent positive net CO₂ efflux (Fig. 14C-13C). Diurnal
 819 patterns became clearer with higher temperatures from May to October (Fig. 14C-13C) and in this period CO₂
 820 fluxes decreased during the day to sometimes reach net negative fluxes (net uptake of CO₂) during and after
 821 midday (Fig. 14C-13C), although the net emissions were also observed in the daytime period (Fig. 14C-13C). The
 822 net negative fluxes can likely be explained by photosynthetic activity of aquatic plants on the surface of the
 823 ditch or by algae in the water column which was measured due to the transparency of the chamber. Using an
 824 opaque chamber instead would likely have resulted in different net CO₂ efflux in daytime. For N₂O, the same

825 pattern as for CH_4 was observed, where flux magnitude across the day fluctuated around zero, except for
 826 January where N_2O fluxes were consistently above zero (Fig. 14D-13D).

827 **3.7.8.3.3 Monthly variability in ditch fluxes**



828
 829 **Figure 14.5:** Monthly summed ditch fluxes of A) CH_4 in $\text{g CH}_4 \text{ m}^{-2}$, B) CO_2 in $\text{g CO}_2 \text{ m}^{-2}$ and C) N_2O in $\text{g N}_2\text{O} \text{ m}^{-2}$ for
 830 the measurement period from February 2022 to January 2023. In A) the blue dashed line is the contribution of
 831 diffusive fluxes and the shaded blue area between the full and dashed blue lines represent the monthly contribution of
 832 ebullition to the total flux. Red and grey dashed lines show the monthly average air (AT) and groundwater
 833 temperature (T_{WTD}) in $^{\circ}\text{C}$, respectively.

835 The monthly sums of CH_4 tend to increase with air temperature, although peak CH_4 emissions (September)
 836 occurred after air temperature peak (July) (Fig. 15A-14A). Diffusive fluxes comprised the major emission
 837 pathway of CH_4 in the ditch (between 21% - 99%), with the contribution from ebullition being highest in March
 838 (55%) and April (78%) (Fig. 15A-14A). Water temperature in the ditch was relatively stable throughout the year,
 839 varying between 5.8 – 10.1 $^{\circ}\text{C}$ being highest from April to November and lowest from December to March.
 840 However, there is little indication of a direct relation between ditch water temperature and net GHG fluxes (Fig.
 841 15A-14A-C).

842 For CO_2 and N_2O , the seasonal pattern is reversed with lowest fluxes during the warmest periods, approaching
 843 net zero or even net negative fluxes (Fig. 15B-14B and C).

844 **4 Data availability**

845 Data for this publication is available for download via <https://doi.org/10.60612/DATADK/BZQ8JE>,
846 <https://dataverse.diee.dk/previewurl.xhtml?token=abda26d4-a430-4830-ad30-fbf5ff1d352e> (Skov Nielsen et al.
847 2025).

848 5 Conclusion

849 The dataset presented here is unique for temperate fens and demonstrates the advantage of using automated
850 GHG measurement systems to resolve temporal and spatial patterns of GHG dynamics in high detail. It
851 represents a full year of data from 2022–2023 and must be considered specific to this period and the location at
852 Vejrumbro. Consequently, it is expected that the annual budget of all GHGs in other years will likely differ due
853 to varying climatic and hydrological conditions.

854 Specifically, the dataset demonstrates how temporal variation in soil hydrology and temperature is linked to the
855 temporal variation of fluxes. Interestingly, the temporal variability of GHG fluxes across the transect appears to
856 be lower than the spatial variation highlighting that spatial variability in hydrology and temperature may not
857 necessarily be the best predictor of flux magnitudes across the transect. The cause of spatial variability in GHG
858 fluxes remains unresolved and does not clearly link directly to either water table depth (WTD), soil temperature,
859 or soil/groundwater chemical parameters.

860 The initial harvest and herbicide application represent ecosystem disturbances that could potentially alter soil
861 biogeochemistry. However, these were conducted months prior to the start of flux measurements, minimizing
862 the direct effect of herbicide. Continued plant removal from inside the collars was necessary for flux
863 measurements, meaning the fluxes may only be regarded as net soil GHG fluxes and not representative of net
864 ecosystem exchange. Excluding vegetation likely influenced measured fluxes of soil respiration (e.g., excluding
865 root exudates) and reduced plant-mediated CH₄ and N₂O emissions, potentially also reducing interannual
866 variability.

867 *Carbon dioxide fluxes:* The magnitude of annual cumulative CO₂ fluxes is in the same range as other studies of
868 temperate fens. Temporal variability is largely governed by the seasonality of WTD and soil temperature (T_{soil}).
869 Soil CO₂ fluxes showed diurnal variability with higher fluxes during midday, where the amplitude between
870 night and day was augmented with T_{soil}.

871 *Nitrous oxide fluxes:* Cumulative soil N₂O fluxes exceed previously reported values for temperate fens at the
872 Vejrumbro site and others. Unlike CO₂, N₂O is emitted largely in pulses related to rapid fluctuations of WTD,
873 which increase in size with T_{soil}, indicating a seasonal regulation of N₂O production by temperature. These
874 measurements suggest an important but difficult-to-capture dynamic of N₂O in peatlands, where hot moments
875 during warm periods determine most of the annual emissions. Soil N₂O fluxes also showed diurnal variability
876 similar to CO₂.

877 *Methane fluxes:* The peat soils across the transect were insignificant sources of CH₄ during the measurement
878 period. This could be linked to deeper WTD (20–40 cm) during summer, a cold wet winter, and the presence of
879 alternative electron acceptors (NO₃⁻, SO₄²⁻, and Fe³⁺), which provide suboptimal conditions for CH₄ production.
880 Vegetation removal may have further impeded CH₄ emissions by restricting plant-mediated pathways. Soil CH₄
881 fluxes did not show diurnal variability.

882 The ditch at the transect was a net source of both N₂O and CO₂, but at magnitudes 27 and 4 times lower than the
883 soil GHG fluxes, respectively. It acted as a CH₄ source, comparable to other ditches in temperate fens. CH₄ was
884 emitted mostly through diffusive emissions from the water surface, with occasional observations of ebullition.

885 This dataset provides a unique opportunity to test hypotheses regarding spatial and temporal patterns of GHG
886 emissions and their drivers in peatlands. It supports the development of models that predict soil GHG fluxes in
887 response to soil temperature and hydrology (WTD), aiding in the prediction of reliable budgets for locations
888 beyond Vejrumbro. We intend to publish this dataset to the research community so that experimentalists and
889 modelers can use it to explore basic hydrological and thermal regulation of GHG fluxes and develop predictive
890 models for spatiotemporal variability.

891 The dataset presented here is unique for temperate fens and demonstrate the advantage of using automated GHG
892 measurements systems to resolve temporal and spatial patterns of GHG dynamics in high detail. The dataset also
893 demonstrate how especially temporal variation of soil hydrology and temperature is linked to the dynamics of
894 fluxes and highlight that spatial variability in hydrology and temperatures not necessarily is the best predictor of
895 flux magnitudes within the site. The cause for the spatial variability of GHG fluxes remains unresolved and do
896 not clearly link directly to either WTD, soil temperature and soil/groundwater chemical parameters.
897 Interestingly it appears that the temporal variability of GHG fluxes across the transect is lower than the spatial
898 variation.

899 The data only represents one full year in 2022-2023 and hence must be considered specific for this period. It
900 must therefore be expected that the annual budget of all GHG's in other years will be different due to other
901 climatic and hydrological conditions.

902 The initial harvest and herbicide application represent ecosystem disturbances that potentially can alter soil
903 biogeochemistry, but they were done months prior to the start of the flux measurements and hence the direct
904 effect of herbicide would be minimal. The continued plant removal from inside collars was necessary for the
905 flux measurements with the consequence that our fluxes may only be regarded as net soil GHG fluxes, and not
906 as being representative of the net ecosystem exchange. Excluding the influence of vegetation have influenced
907 the measured fluxes of soil respiration (e.g. excluding root exudates etc.) and reduced plant mediated CH₄ and
908 N₂O emissions and lowered most likely also reduced interannual variability. However, the data set represents a
909 unique ability to continue to develop models that predict the soil GHG fluxes in response to soil temperature and
910 hydrology (WTD) that can aid in prediction of reliable budgets for sites.

911 The measurements of the soil GHG fluxes show that the magnitude of annual cumulative CO₂ fluxes are in the
912 same range as in other studies of temperate fens, and that temporal variability are largely governed by the
913 seasonality of WTD and ST. However, spatial variation of cumulative fluxes for all GHG were not directly
914 related to WTD levels, contradicting the general assumption that WTD is the primary driver of GHG emissions.
915 Cumulative soil N₂O fluxes exceed what has been previously reported for temperate fens, but show similar
916 seasonal regulation by ST. However, in contrast to soil CO₂ fluxes, soil N₂O is emitted largely in pulses related
917 to rapid fluctuations of WTD that increase in size with temperature. These measurements therefore point to an
918 important, but difficult to capture dynamic of N₂O in peatlands where hot moments during the warm periods
919 determine most of the annual emissions. A likely cause for the high soil N₂O emissions could be a combination

920 of leaching of inorganic nitrogen from surrounding agricultural fields and release of organic N from the
921 decomposing peat. The site was during the measurement period an insignificant source of soil CH₄, which is
922 likely due to the well drained summer period, a cold wet winter and presence of the major electron acceptors
923 (NO₃⁻, SO₄²⁻ and Fe³⁺), providing suboptimal conditions for CH₄ production. However, it cannot be ruled out
924 that the vegetation removal impeded CH₄ emissions, as we effectively restricted plant mediated CH₄ emissions.
925 Therefore, caution should be taken when comparing the CH₄ flux data to other drained peatlands. Soil CO₂ and
926 N₂O fluxes both showed diurnal variability with higher fluxes during midday where the amplitude between
927 night and day was augmented with ST. This was not observed for soil CH₄ fluxes. The ditch at the site was a net
928 source of both N₂O and CO₂, but at rates 27 and 4 times lower than the soil GHG fluxes respectively. However,
929 the ditch acted as a CH₄ source mostly comprised of diffusive emissions from the water surface, but with
930 observations of ebullition.

931 We wish to publish this dataset to the research community with the intention that experimentalists and modellers
932 can use the data to test hypothesis on basic hydrological and thermal regulation of GHG fluxes and develop
933 models to predict spatiotemporal variability of the GHG fluxes.

934 Competing interests

935 The authors declare that they have no conflict of interest.

936 Author contributions

937 JRC, PEL and KSL designed the experiment and carried them out. ASN performed flux calculation and quality
938 checking. RJP and PEL installed the equipment for groundwater measurements. All authors contributed to
939 writing of this manuscript.

940 Acknowledgements

941 The measurements are the results of the RePeat (grant nr. 33010-NIFA-19-724), INSURE and ReWet (grant nr.
942 5229-0002b) projects hosted by University of Copenhagen and Aarhus University. ReWet is part of the Danish
943 roadmap for research infrastructure funded by The Danish Agency for Science and Higher Education. INSURE
944 was part of EJP Soil and received funding from the European Union's Horizon 2020 research and innovation
945 programme under the grant agreement no. 862695.

946 References

- 947 Anthony, T. L. and Silver, W. L.: Hot spots and hot moments of greenhouse gas emissions in agricultural
948 peatlands, *Biogeochemistry*, 167, 461–477, <https://doi.org/10.1007/s10533-023-01095-y>, 2023.
- 949 Askaer, L., Elberling, B., Friberg, T., Jørgensen, C. J., and Hansen, B. U.: Plant-mediated CH₄ transport
950 and C gas dynamics quantified in-situ in a Phalaris arundinacea-dominant wetland, *Plant Soil*, 343, 287–
951 301, <https://doi.org/10.1007/s11104-011-0718-x>, 2011.
- 952 Boonman, J., Buzacott, A. J. V., van den Berg, M., van Huissteden, C., and van der Velde, Y.: Transparent
953 automated CO₂ flux chambers reveal spatial and temporal patterns of net carbon fluxes from managed
954 peatlands, *Ecol Indic*, 164, 112121, <https://doi.org/10.1016/j.ecolind.2024.112121>, 2024.
- 955 Brændholt, A., Steenberg Larsen, K., Ibrom, A., and Pilegaard, K.: Overestimation of closed-chamber soil
956 CO₂ effluxes at low atmospheric turbulence, *Biogeosciences*, 14, 1603–1616, <https://doi.org/10.5194/bg-14-1603-2017>, 2017.

- 958 Bridgman, S. D., Cadillo-Quiroz, H., Keller, J. K., and Zhuang, Q.: Methane emissions from wetlands:
959 biogeochemical, microbial, and modeling perspectives from local to global scales, *Glob Chang Biol*, 19,
960 1325–1346, <https://doi.org/10.1111/gcb.12131>, 2013.
- 961 Christiansen, J. R., Outhwaite, J., and Smukler, S. M.: Comparison of CO₂, CH₄ and N₂O soil-atmosphere
962 exchange measured in static chambers with cavity ring-down spectroscopy and gas chromatography,
963 *Agric For Meteorol*, 211–212, 48–57, <https://doi.org/10.1016/j.agrformet.2015.06.004>, 2015.
- 964 Christiansen, J. R., Levy-Booth, D., Prescott, C. E., and Grayston, S. J.: Microbial and Environmental
965 Controls of Methane Fluxes Along a Soil Moisture Gradient in a Pacific Coastal Temperate Rainforest,
966 *Ecosystems*, 19, 1255–1270, <https://doi.org/10.1007/s10021-016-0003-1>, 2016.
- 967 Evans, C. D., Peacock, M., Baird, A. J., Artz, R. R. E., Burden, A., Callaghan, N., Chapman, P. J.,
968 Cooper, H. M., Coyle, M., Craig, E., Cumming, A., Dixon, S., Gauci, V., Grayson, R. P., Helfter, C.,
969 Heppell, C. M., Holden, J., Jones, D. L., Kaduk, J., Levy, P., Matthews, R., McNamara, N. P.,
970 Misselbrook, T., Oakley, S., Page, S. E., Rayment, M., Ridley, L. M., Stanley, K. M., Williamson, J. L.,
971 Worrall, F., and Morrison, R.: Overriding water table control on managed peatland greenhouse gas
972 emissions, *Nature*, 593, 548–552, <https://doi.org/10.1038/s41586-021-03523-1>, 2021.
- 973 Jørgensen, C. J., Struwe, S., and Elberling, B.: Temporal trends in N₂O flux dynamics in a Danish wetland
974 - effects of plant-mediated gas transport of N₂O and O₂ following changes in water level and soil mineral-
975 N availability, *Glob Chang Biol*, 18, 210–222, <https://doi.org/10.1111/j.1365-2486.2011.02485.x>, 2012.
- 976 Jørgensen, M. S., Plauborg, F., and Kørup, K.: Climate normal for Foulum 1991–2020, Aarhus University,
977 2023.
- 978 Kandel, T. P., Lærke, P. E., and Elsgaard, L.: Annual emissions of CO₂, CH₄ and N₂O from a temperate
979 peat bog: Comparison of an undrained and four drained sites under permanent grass and arable crop
980 rotations with cereals and potato, *Agric For Meteorol*, 256–257, 470–481,
981 <https://doi.org/10.1016/j.agrformet.2018.03.021>, 2018.
- 982 Koch, J., Elsgaard, L., Greve, M. H., Gyldenkærne, S., Hermansen, C., Levin, G., Wu, S., and Stisen, S.:
983 Water-table-driven greenhouse gas emission estimates guide peatland restoration at national scale,
984 *Biogeosciences*, 20, 2387–2403, <https://doi.org/10.5194/bg-20-2387-2023>, 2023.
- 985 Köhn, D., Welpelo, C., Günther, A., and Jurasinski, G.: Drainage Ditches Contribute Considerably to the
986 CH₄ Budget of a Drained and a Rewetted Temperate Fen, *Wetlands*, 41, 71,
987 <https://doi.org/10.1007/s13157-021-01465-y>, 2021.
- 988 Kroon, P. S., Hensen, a., Bulk, W. C. M., Jongejan, P. a. C., and Vermeulen, a. T.: The importance of
989 reducing the systematic error due to non-linearity in N₂O flux measurements by static chambers, *Nutr
990 Cycl Agroecosyst*, 82, 175–186, <https://doi.org/10.1007/s10705-008-9179-x>, 2008.
- 991 Nguyen, D. B., Rose, M. T., Rose, T. J., Morris, S. G., and van Zwieten, L.: Impact of glyphosate on soil
992 microbial biomass and respiration: A meta-analysis, *Soil Biol Biochem*, 92, 50–57,
993 <https://doi.org/https://doi.org/10.1016/j.soilbio.2015.09.014>, 2016.
- 994 Nielsen, C. K., Liu, W., Koppelgaard, M., and Laerke, P. E.: To Harvest or not to Harvest: Management
995 Intensity did not Affect Greenhouse Gas Balances of Phalaris Arundinacea Paludiculture, *Wetlands*, 44,
996 79, <https://doi.org/10.1007/s13157-024-01830-7>, 2024.
- 997 Padilla, J. T. and Selim, H. M.: Environmental behavior of glyphosate in soils, *Advances in Agronomy*,
998 159, 1–34, <https://doi.org/10.1016/BS.AGRON.2019.07.005>, 2020.
- 999 Peacock, M., Audet, J., Bastviken, D., Cook, S., Evans, C. D., Grinham, A., Holgerson, M. A., Högbom,
1000 L., Pickard, A. E., Zieliński, P., and Futter, M. N.: Small artificial waterbodies are widespread and
1001 persistent emitters of methane and carbon dioxide, *Glob Chang Biol*, 27, 5109–5123,
1002 <https://doi.org/10.1111/gcb.15762>, 2021.

- 1003 Pedersen, A. R., Petersen, S. O., and Schelde, K.: A comprehensive approach to soil-atmosphere trace-gas
1004 flux estimation with static chambers, *Eur J Soil Sci*, 61, 888–902, <https://doi.org/10.1111/j.1365-2389.2010.01291.x>, 2010.
- 1006 Pihlatie, M. K., Christiansen, J. R., Aaltonen, H., Korhonen, J. F. J., Nordbo, A., Rasilo, T., Benanti, G.,
1007 Giebels, M., Helmy, M., Sheehy, J., Jones, S., Juszczak, R., Klefth, R., Lobo-do-Vale, R., Rosa, A. P.,
1008 Schreiber, P., Serça, D., Vicca, S., Wolf, B., and Pumpanen, J.: Comparison of static chambers to measure
1009 CH₄ emissions from soils, *Agric For Meteorol*, 171–172, 124–136,
1010 <https://doi.org/10.1016/j.agrformet.2012.11.008>, 2013.
- 1011 Prairie, Y. T. and del Giorgio, P. A.: A new pathway of freshwater methane emissions and the putative
1012 importance of microbubbles, *Inland Waters*, 3, 311–320, <https://doi.org/10.5268/IW-3.3.542>, 2013.
- 1013 Pullens, J. W. M., Abalos, D., Petersen, S. O., and Pedersen, A. R.: Identifying criteria for greenhouse gas
1014 flux estimation with automatic and manual chambers: A case study for N₂O, *Eur J Soil Sci*, 74,
1015 <https://doi.org/10.1111/ejss.13340>, 2023.
- 1016 Reza Mashhadi, S., Grombacher, D., Zak, D., Erik Lærke, P., Estrup Andersen, H., Christian Hoffmann,
1017 C., and Jes Petersen, R.: Borehole nuclear magnetic resonance as a promising 3D mapping tool in peatland
1018 studies, *Geoderma*, 443, 116814, <https://doi.org/10.1016/j.geoderma.2024.116814>, 2024.
- 1019 Rheault, K., Christiansen, J. R., and Larsen, K. S.: goFlux: A user-friendly way to calculate GHG fluxes
1020 yourself, regardless of user experience, *J Open Source Softw*, 9, 6393,
1021 <https://doi.org/10.21105/joss.06393>, 2024.
- 1022 Sø, J. S., Sand-Jensen, K., Martinsen, K. T., Polauke, E., Kjær, J. E., Reitzel, K., and Kragh, T.: Methane
1023 and carbon dioxide fluxes at high spatiotemporal resolution from a small temperate lake, *Science of The
1024 Total Environment*, 878, 162895, <https://doi.org/10.1016/j.scitotenv.2023.162895>, 2023.
- 1025 Tiemeyer, B., Freibauer, A., Borraz, E. A., Augustin, J., Bechtold, M., Beetz, S., Beyer, C., Ebli, M.,
1026 Eickenscheidt, T., Fiedler, S., Förster, C., Gensior, A., Giebels, M., Glatzel, S., Heinichen, J., Hoffmann,
1027 M., Höper, H., Jurasiński, G., Laggner, A., Leiber-Sauheitl, K., Peichl-Brak, M., and Drösler, M.: A new
1028 methodology for organic soils in national greenhouse gas inventories: Data synthesis, derivation and
1029 application, *Ecol Indic*, 109, 105838, <https://doi.org/10.1016/j.ecolind.2019.105838>, 2020.
- 1030 Vroom, R. J. E., van den Berg, M., Pangala, S. R., van der Scheer, O. E., and Sorrell, B. K.: Physiological
1031 processes affecting methane transport by wetland vegetation – A review, *Aquat Bot*, 182, 103547,
1032 <https://doi.org/https://doi.org/10.1016/j.aquabot.2022.103547>, 2022.
- 1033 Wik, M., Varner, R. K., Anthony, K. W., MacIntyre, S., and Bastviken, D.: Climate-sensitive northern
1034 lakes and ponds are critical components of methane release, *Nat Geosci*, 9, 99–105,
1035 <https://doi.org/10.1038/ngeo2578>, 2016.
- 1036 Wilson, S. J., Bond-Lamberty, B., Noyce, G., Bittencourt Peixoto, R., and Megonigal, J. P.: fluxfinder: An
1037 R Package for Reproducible Calculation and Initial Processing of Greenhouse Gas Fluxes From Static
1038 Chamber Measurements, *J Geophys Res Biogeosci*, 129, <https://doi.org/10.1029/2024JG008208>, 2024.
- 1039